# INELASTIC ELECTRON SCATTERING FORM FACTORS FOR THE EXCITATION OF LOW - LYING LEVELS IN SOME 2p - 1f SHELL NUCLEI

*A Thesis Submitted*
in Partial Fulfilment of the Requirements
for the Degree of

DOCTOR OF PHILOSOPHY

*By*

GOUTAM MUKHOPADHYAY

*to the*

DEPARTMENT OF PHYSICS
INDIAN INSTITUTE OF TECHNOLOGY, KANPUR

DECEMBER, 1985

PHY-1985-D-MUK-INE

To

My Parents

CERTIFICATE

Certified that the work presented in this thesis entitled, "Inelastic Electron Scattering Form Factors for the Excitation of Low-Lying Levels in some 2p-1f Shell Nuclei", by Mr. Goutam Mukhopadhyay has been carried out under my supervision and that this has not been submitted elsewhere for a degree.

December, 1985.

S.K. Sharma

(S.K. SHARMA)
Assistant Professor
Department of Physics
Indian Institute of Technology, Kanpur
KANPUR-208016 (India)

## ACKNOWLEDGEMENTS

I express my sincerest thanks and deepest sense of gratitude and indebtedness to my supervisor, Dr. Sateesh Kumar Sharma for his invaluable guidance during the course of my research work. Working with him was actually a learning experience. I am indebted to him not only for his guidance and help awarded for the present work but also for bringing me out of the maze of present day research and invoking in me a keen interest in microscopic many-body Physics. I shall ever be grateful to him for his untiring help, personal interest, helpful discussions, fruitful assistance and affectionate behaviour throughout the span of this work.

I am also sincerely thankful to several other faculty members of the Department of Physics, Indian Institute of Technology, Kanpur, especially Prof. Y.R. Waghmare, Prof. R.M. Singru, Dr. A.P. Shukla and Dr. Vijay Singh for their interests shown in this work. Helps and suggestions from them from time to time are deeply appreciated.

The calculations reported in this thesis have been carried out at the DEC-1090 timesharing computer, IIT Kanpur. I acknowledge gratefully the help and assistance given by the staff members of the Computer Centre, IIT Kanpur.

It is a great pleasure to thank my senior colleague Dr. Prakash Narayan Tripathi, Reader, VSSD College, Kanpur, as well as my friends Dr. Dinakar Kanjilal, Dr. M.M. Sharma, Mr. Pradeep Khowash, Mr. Buddhadeb Ghosh, Mr. Subodh Godre and Mr. P.K. Raina for their helps and cooperations during the course of this work.

I thank Mr. U.S. Misra for typing out the thesis skilfully and accurately, Mr. R.K. Bajpai for tracing out the figures beautifully and Mr. Hrishikesh Panda for a neat and efficient cyclostyling of the pages.

Last but not the least, I am grateful to Mrs. Kajal Mukherjee for her warm and untiring encouragements.

TABLE OF CONTENTS

# LIST OF TABLES

# LIST OF FIGURES

SYNOPSIS

G. MUKHOPADHYAY

Ph.D. (Physics)
Indian Institute of Technology Kanpur

SEPTEMBER 1985

# INELASTIC ELECTRON SCATTERING FORM FACTORS FOR THE EXCITATION OF LOW-LYING LEVELS IN SOME 2p-1f SHELL NUCLEI

Inelastic electron scattering is a powerful method for investigating nuclear structure. By measuring the cross-section for the scattered electrons, one can determine the Fourier transforms of the nuclear charge and current densities between the initial and the final nuclear states. In comparison with ordinary gamma transition the momentum-transfer dependence of the nuclear matrix elements contains information about the spatial structure of the nuclear ground and excited states and can therefore give us a good test of the nuclear wave functions and the transition operators used in the theoretical models.

Some recent inelastic electron scattering experiments presented valuable data on the $0^+_{g.s.} \rightarrow 2^+_1$ as well as $0^+_{g.s.} \rightarrow 2^+_2$ transitions in several 2p-1f shell nuclei. Within a measured momentum transfer range upto $q_{eff} \sim 2$ fm$^{-1}$, the C2 form factors involving $0^+_{g.s.} \rightarrow 2^+_1$ transitions are characcterized by two peaks appearing at $q_{eff} \sim 0.7$ fm$^{-1}$ and at $q_{eff} \sim 1.7$ fm$^{-1}$. Although the qualitative features of the

form factors associated with the $0^+_{g.s.} \longrightarrow 2^+_2$ transitions are quite similar to those of the observed form factors for the $0^+_{g.s.} \longrightarrow 2^+_1$ transitions, the magnitudes of $|F|^2$ for the former transitions are smaller by an order of magnitude than those for the latter.

In a recent shell-model study the C2 form factors for some Ti, Cr and Fe isotopes were calculated in terms of wave functions resulting from empirical effective interactions operating in a restricted valence space involving the $f^n_{7/2} + f^{n-1}_{7/2}\ p_{3/2}$ configurations. The use of the truncated shell model wavefunctions necessitated the use of highly mass-dependent effective charges for the interpretation of available data.

In the present work we show that the angular momentum projected Hartree-Fock-Bogoliubov (PHFB) wave functions resulting from realistic effective interactions operating in the full 2p-1f shell permit a consistent microscopic description of the available experimental data on form factors in terms of nearly constant effective charges. To our knowledge the use of PHFB wave functions to interpret the available form factor data has not been reported so far.

Chapter I presents the background and the genesis of the topics that we have selected for investigation in the present work.

The choice of effective two body interaction is a crucial element of the calculations involving HF or HFB wave

functions. In Chapter II we have tested the various available effective interactions in the 2p-1f shell in terms of their PHFB estimates for the subshell occupation numbers for protons and neutrons. The effective interaction providing the best agreement between the available and the calculated subshell occupation numbers is later used in the subsequent chapters for the detailed calculation of the inelastic electron scattering form factors.

In Chapter III we present the calculation of the inelastic electron scattering form factors for the excitation of $2_1^+$ states in some even-even 2p-1f shell nuclei in the PHFB framework using a slightly modified version of the Kuo Brown effective interaction. Apart from the C2 form factors we have also calculated the static quadrupole moments, $Q_{2^+}$, and the reduced transition probabilities for E2 transitions, $B(E2;\ 0^+ \longrightarrow 2_1^+)$, in these nuclei. In keen contrast with the results obtained in the shell model calculations involving $f_{7/2}^n + f_{7/2}^{n-1} p_{3/2}$ configurations, it is seen that the use of the self-consistent PHFB wave functions leads not only to a significant overall improvement in the calculated form factors, but also obviates the necessity of using widely different effective charges for various nuclei. In view of the intractibility of large-scale shell model calculation in the 2p-1f shell nuclei, the method employed in the present work is expected to provide a reliable alternative for obtaining a reasonably accurate microscopic description of the

observed data on C2 form factors.

In Chapter IV we present the calculation of the inelastic electron scattering form factors for the excitation of the $2_2^+$ states in the even-even 2p-1f shell nuclei $^{48}$Ti and $^{50}$Cr in the PHFB framework using the modified Kuo-Brown effective interaction. It is seen that the use of the yrast and yrare states with $J^\pi = 0^+, 2^+$ projected from the self-consistent prolate and oblate intrinsic shapes permits a reasonably accurate description of the observed form factor data involving the $0^+_{g.s.} \longrightarrow 2^+_2$ transitions.

As mentioned earlier, an important feature that characterizes the observed form factors for the $0^+_{g.s.} \longrightarrow 2^+_2$ transitions in the nuclei $^{48}$Ti and $^{50}$Cr is their reduced magnitude, by roughly an order, compared to those for the $0^+_{g.s.} \longrightarrow 2^+_1$ transitions. Present calculation offers a qualitative understanding of this feature of the $0^+_{g.s.} \rightarrow 2^+_2$ transitions in terms of the reduced overlaps between the initial ($0^+_{g.s.}$) and the final ($2^+_2$) states due to their different intrinsic parentage.

Finally in Chapter V we summarize the results and discuss some possible extensions of the present work.

# CHAPTER I

## INTRODUCTION

The elastic as well as inelastic electron scattering provides an excellent tool for exploring nuclear structure for a variety of reasons[1,2]. The principal reason for the usefulness of the electron as a probe is that the interaction between the electron and the nucleus is the well-understood electromagnetic interaction that is described by an exact theory-quantum electrodynamics. As a consequence of this, the nuclear properties can be related to the electron scattering data in an unambiguous, quantitative way. Another feature that favours the choice of the electron as a probe is the weakness of the electromagnetic interaction; the coupling constant for the electromagnetic interaction is much smaller than the strength of the nuclear force. An electron, therefore, probes the nucleus gently, causing very little disturbance in the process.

Considering the excitation of nuclear levels, the superiority of inelastic electron scattering over other methods involving electromagnetic interactions-and here we may cite photoabsorption — lies in the separate variability of energy and momentum transfer. This allows us to map inelastic form factors for various nuclear excitations as functions of momentum transfer q.

Here we must also mention some of the inherent shortcomings that are associated with the electron scattering experiments. Due to its small mass, the electron may be easily deflected, and most of such deflections usually result in radiation. This leads to strong background to the excitation cross section. A theoretical drawback is also related to the fact that, due to the strong distortion of the electron wavefunction by the Coulomb interaction, it becomes necessary to go beyond the plane-wave Born approximation (PWBA) for carrying out an analysis of inelastic scattering experiments involving heavy nuclei ($Z > 20$).

Within the framework of PWBA applied to the electroexcitation of low-lying nuclear levels of light nuclei, a measurement of the cross section for the scattered electron permits one to obtain the Fourier transforms of the nuclear charge and current densities between the initial and final states involved in the transition. The momentum-transfer dependence of the nuclear matrix elements contains information about the spatial structure of the nuclear ground and excited states and, therefore, provides us with a good test of the nuclear wavefunctions.

A number of recent inelastic electron scattering experiments have provided valuable data on the $0^+ \rightarrow 2^+_{1,2,3}$ transitions in several 2p-1f shell nuclei[3-7]. Some of the salient features of the available form factor data covering

the range $q_{eff}$ = 0.1-2.0 $fm^{-1}$ are the following:

i) The form factors for the $0^+ \rightarrow 2^+_1$ transitions are characterized by two peaks appearing at $q_{eff} \sim 0.7$, 1.7 $fm^{-1}$. The form factors display a minimum at $q_{eff} \sim 1.3$ $fm^{-1}$.

ii) The qualitative features of the form factors associated with the $0^+ \rightarrow 2^+_{2,3}$ transitions are quite similar to those of the observed form factors for the $0^+ \rightarrow 2^+_1$ transitions the magnitudes of the form factors for the former transitions are, however, smaller by an order of magnitude than those for the latter.

The work presented in this thesis is motivated by a desire to provide a consistent microscopic description of the available experimental data[3-7] on the electroexcitation of low-lying levels in the 2p-1f shell nuclei. This is sought to be achieved by calculating the form factors in terms of the angular momentum projected Hartree-Fock-Bogoliubov (HFB) wave functions[8] resulting from the realistic effective interactions operating in the valence space spanned by the ($1f_{7/2}$, $2p_{3/2}$, $2p_{1/2}$, $1f_{5/2}$) orbits. A calculation of the form factors in terms of exact shell model wavefunctions generated within the ($1f_{7/2}$, $2p_{3/2}$, $2p_{1/2}$, $1f_{5/2}$)$^n$ space is not tractable for the nuclei in the mass range A = 40-80 since the dimensionalities of the relevant shell model matrices are prohibitively large. In

this context, the method outlined in the present work is expected to provide a reliable alternative for obtaining a reasonably accurate microscopic description of the observed form factors.

Variational wavefunctions for several valence particles occupying reasonably large configuration spaces usually depend quite sensitively on the effective interaction employed in the calculation. We have, therefore, first examined, in Chapter II, the suitability of various available effective interactions by comparing the ground state subshell occupation numbers resulting from these interactions with the experiments[9]. It turns out that a slightly modified version of the Kuo-Brown (KB) effective interaction[10] suggested by McGrory, Wildenthal, and Halbert[11] provides reasonably good agreement between the available and the calculated subshell occupation numbers in several 2p-1f shell nuclei. This effective interaction, hereafter labelled the MWH interaction, has been employed in subsequent Chapters for the calculation of inelastic electron scattering form factors. In Chapter II we have also presented a comparative study of the projected HFB method as well as the spectral distribution method developed by French and co-workers[12,13] vis-à-vis their predictions for the subshell occupation numbers.

We next discuss in Chapter III the calculation[14] of the form factors for the $0^+ \rightarrow 2_1^+$ transitions in some doubly

even Ti, Cr and Fe isotopes in terms of projected HFB wavefunctions resulting from the MWH effective interaction. The quadrupole moments of the first excited $2^+$ states as well as the reduced transition probabilities for E2 transitions, $B(E2; 0^+ \rightarrow 2_1^+)$, are also discussed in connection with the form factors. Recently Iwamoto et al.[7] had carried out a shell model study of the $0^+ \rightarrow 2_1^+$ form factors in terms of wave functions resulting from empirical effective interactions operating in the valence space of the $(1f_{7/2}^n + 1f_{7/2}^{n-1}2p_{3/2})$ configurations. The calculation required proton and neutron effective charges possessing relatively strong number dependence for a reasonably successful interpretation of the available data. Our calculations involving an unrestricted valence space spanned by the $(1f_{7/2}, 2p_{3/2}, 2p_{1/2}, 1f_{5/2})^n$ configurations demonstrate that the use of the self-consistent projected HFB wavefunctions obviates the necessity of employing widely different effective charges for various nuclei, in addition to providing significant overall improvement in the calculated form factors.

In Chapter IV we present the calculation[15] of the inelastic electron scattering form factors associated with the $0^+ \rightarrow 2_2^+$ transitions in the nuclei ($^{48}Ti$, $^{50}Cr$, $^{54}Fe$) and the $0^+ \rightarrow 2_3^+$ transition in the nucleus $^{56}Fe$. The calculations of the form factors involving the non-yrast $2^+$ levels employ the same overall calculational framework as well as the set of input parameters - the effective two-body

interaction as well as the spherical single-particle energies - as the one employed in Chapter III. Iwamoto et al.[7] have sometime ago also discussed the $0^+ \rightarrow 2_2^+$ form factors in some doubly even Ti and Cr isotopes employing the configuration space $(f_{7/2}^n + f_{7/2}^{n-1} p_{3/2})$ in conjunction with the empirical effective interactions given by Oda et al.[16] as well as by Yokoyama et al.[17]. The earlier calculation brought out the sensitivity of the restricted shell model results for the $0^+ \rightarrow 2_2^+$ form factors towards the choice of the effective interaction; the calculated results displayed large variation in going from one interaction to another. Also, none of the two interactions provided acceptable simultaneous agreement for the $0^+ \rightarrow 2_1^+$ as well as $0^+ \rightarrow 2_2^+$ transitions. The calculations presented here demonstrate that a reasonably satisfactory interpretation of the available form factor data involving both the yrast as well as non-yrast $J^\pi = 2^+$ states can be provided in terms of the prolate and oblate variational states resulting from the MWH interaction.

As pointed out earlier, the observed form factors for the $0^+ \rightarrow 2_{1,2}^+$ transitions in the 2p-1f shell nuclei are characterized by the property that $[|F(q)|^2(0^+ \rightarrow 2_1^+)/|F(q)|^2(0^+ \rightarrow 2_2^+)] \simeq 10$. The calculations presented in Chapter IV provide a qualitative understanding of this feature of the $0^+ \rightarrow 2_2^+$ form factors in terms of the reduced overlap between the initial and the final states due to

their different intrinsic parentage.

Finally, in Chapter V we summarize the results obtained in, and wisdom gained from Chapters II, III and IV.

## REFERENCES


1. T. de Forest and J. Walecka, Advances in Physics 15, 1 (1966).

2. H. Überall, Electron Scattering From Complex Nuclei (Academic, New York, 1971).

3. J. Heisenberg, J.S. McCarthy and I. Sick, Nucl. Phys. A164, 353 (1971).

4. K. Hosoyama et al., Res. Rep. Nucl. Sc. (Tohoku University). 7, 279 (1974); 8, 55 (1975).

5. J.W. Lightbody, Jr. et al., Bull. Am. Phys. Soc. 20, 568 (1975).

6. K. Hosoyama et al., Res. Rep. Nucl. Sc. (Tohoku University) 11, 1 (1978).

7. T. Iwamoto, H. Horie and A. Yokoyama, Phys. Rev. C25, 658 (1982).

8. A.L. Goodman, in Advances in Nuclear Physics, edited by J.W. Negele and E. Vogt (Plenum, New York, 1979), Vol.11,

9. G. Mukherjee and S.K. Sharma, Phys. Rev. C33 (in press).

10. T.T.S. Kuo and G.E. Brown, Nucl. Phys. A114, 241 (1968).

11. J.B. McGrory, B.H. Wildenthal and E.C. Halbert, Phys. Rev. C2, 186 (1970); S.K. Sharma and K.H. Bhatt, Phys. Rev. Letters 30, 620 (1973).

12. J.B. French, in Proceedings of the International School of Physics "Enrico Fermi", Course XXXVI, edited by C. Bloch (Academic, New York, 1966), p. 278.

13. F.S. Chang, J.B. French, and T.H. Thio, Ann. Phys. (NY) 66, 137 (1971).

14. G. Mukherjee and S.K. Sharma, Phys. Rev. C29, 2101 (1984).

15. G. Mukherjee and S.K. Sharma, Phys. Rev. C31, 689 (1985).

16. T. Oda, K. Muto and H. Horie, Lett. Nuovo Cimento 18, 549 (1977).

17. A. Yokoyama, T. Oda and H. Horie, Prog. Theor. Phys. 60, 427 (1978).

# CHAPTER II

## PROTON-NEUTRON OCCUPANCIES OF SPHERICAL SHELLS IN THE GROUND STATES OF SOME DOUBLY EVEN NUCLEI WITH A = 46-70 AND THE EFFECTIVE INTERACTIONS OPERATIVE IN THE 2p-1f SHELL

### II.1 Introduction

The expectation value of the subshell occupancy operator is one of the simplest measurable dynamical quantities in the ground state of a nucleus. The measured values of the subshell occupation numbers provide a direct test of the nuclear wave functions involved in the microscopic description of the ground state.

Recent years have witnessed considerable increase in our knowledge of the spectroscopic factors for pickup and stripping reactions involving various 2p-1f shell nuclei[1-6]. The measured spectroscopic factors can be related to the subshell occupation numbers by using non-energy-weighted sum rules[7].

The calculations presented in this chapter are intended to examine the suitability of various effective interactions operative in the 2p-1f shell from the point of view of detailed spectroscopic calculations by comparing the ground state occupancies generated by these interactions with the experimental values.

Unlike in the case of the 2s-1d shell, a calculation of the subshell occupation numbers in terms of the exact shell model wave functions is not feasible in the context of

the 2p-1f shell nuclei; the dimensionalities of the Hamiltonian matrices involved are prohibitively large. Furthermore, the collective nature of the observed properties of the nuclei with $46 \leq A \leq 70$ necessitates the involvement of the full 2p-1f valence space, and any calculation employing a truncation of the shell model space is not expected to give accurate results.

The Hartree-Fock (HF) or the Hartree-Fock-Bogoliubov (HFB) approaches are a priori quite suited for the calculation of subshell occupation numbers for the ground states resulting from a given effective interaction[8]. The requirement of the minimization of energy for the HF or HFB ansatz of the variational wavefunction is connected primarily with the extraction of the one-body field. The lowest-energy HF or HFB intrinsic state, therefore, corresponds to the optimum single-particle field (resulting from two-body interactions) appropriate for the ground states. This single-particle field in turn provides the best set of (single-particle) wavefunctions for calculating the expectation values of various one-body operators in the ground states.

Kota and Potbhare[9] have sometime ago reported the calculation of the ground state energies and the subshell occupation numbers for several 2p-1f shell nuclei in the framework of the spectral distribution method developed by French and coworkers[10,11]. The occupation numbers resulting from a number of effective interactions in the 2p-1f shell

were compared. However, it turns out that the ground states in various 2p-1f shell nuclei are usually more than five widths ($\sigma$) away from the centroid of the energy distributions. This constrains severely the usefulness of the spectral distribution method involving just the first two moments of the Hamiltonian; the results obtained via the spectral distribution methods therefore become very sensitive towards the higher-order shape correction to the configuration level density.

We have also presented in this chapter a comparison of the subshell occupation numbers resulting from the projected Hartree-Fock-Bogoliubov (PHFB) and the spectral distribution methods employing effective interactions with known spectroscopic properties; the comparison permits an assessment of the relative efficacy of the PHFB approach.

Section II.2 presents the calculational framework. A brief outline of the HFB method as well as the technique of angular momentum projection as applied to the calculation of the subshell occupation numbers are presented. In section II.3 we discuss the theoretical results and their comparison with the available data. Finally section II.4 contains some concluding remarks.

## II.2 Calculational Framework

### II.2.1 The Hartree-Fock-Bogoliubov (HFB) Method

Consider the shell model Hamiltonian of the nucleus under consideration

$$H = \sum_{\alpha} \langle \alpha | \varepsilon | \alpha \rangle a_{\alpha}^{\dagger} a_{\alpha} + (1/4) \sum_{\alpha\beta\gamma\delta} \langle \alpha\beta | v_A | \gamma\delta \rangle \, a_{\alpha}^{\dagger} a_{\beta}^{\dagger} a_{\delta} a_{\gamma} \quad , \qquad (II.1)$$

where $\varepsilon_\alpha$ are the spherical single-particle energies and $\langle \alpha\beta | v_A | \gamma\delta \rangle$ is the antisymmetrized matrix element of an effective interaction. Here $a_\alpha^\dagger$ and $a_\alpha$ are the creation and annihilation operators in the spherical basis $|\alpha\rangle$. We wish to obtain a transformation from particle coordinates to quasiparticle coordinates such that the quasiparticles are relatively weakly interacting:

$$H = E_o + H_{qp} + H_{qp\text{-}int} \quad , \qquad (II.2)$$

where $E_o$ is the energy of the quasiparticle vacuum, $H_{qp}$ describes the elementary quasiparticle excitations, and $H_{qp\text{-}int}$ is a (hopefully) weak interaction between the quasiparticles.

The Hamiltonian $(E_o + H_{qp})$ may not, in general, preserve all the symmetries of H. In HFB one imposes constraints via the use of Lagrange multipliers such that some of the observables possess desired expectation values. More specifically, we have

$$H' = H - \lambda_\pi N_\pi - \lambda_\nu N_\nu \quad , \qquad (II.3)$$

where the Lagrange multipliers are chosen so that the number operators $N_\pi = \sum_\alpha a^\dagger_{\alpha\pi} a_{\alpha\pi}$ and $N_\nu = \sum_\alpha a^\dagger_{\alpha\nu} a_{\alpha\nu}$ possess the expectation values

$$\langle \Phi_o | N_\pi | \Phi_o \rangle = Z, \langle \Phi_o | N_\nu | \Phi_o \rangle = A-Z \quad . \qquad (II.4)$$

In HFB theory one considers the general Bogoliubov transformation

$$q^\dagger_\alpha = \sum_\beta (U_{\alpha\beta} a^\dagger_\beta + V_{\alpha\beta} a_\beta) \quad . \qquad (II.5)$$

Here U and V are NxN complex matrices in a basis spanned by N single-particle states. The 2Nx2N linear transformation

$$\begin{pmatrix} q^\dagger \\ q \end{pmatrix} = \begin{pmatrix} U & V \\ V^* & U^* \end{pmatrix} \begin{pmatrix} a^\dagger \\ a \end{pmatrix} \quad , \qquad (II.6)$$

is unitary. Writing

$$M = \begin{pmatrix} U & V \\ V^* & U^* \end{pmatrix} \quad , \qquad (II.7)$$

the unitarity conditions $MM^\dagger = M^\dagger M = I$ lead to the relations

$$UU^\dagger + VV^\dagger = U^\dagger U + \tilde{V} V^* = I, \quad U\tilde{V} + V\tilde{U} = U^\dagger V + \tilde{V} U^* = 0, \qquad (II.8)$$

where $U^\dagger$, $\tilde{U}$ and $U^*$ denote, respectively, the adjoint, transpose and the complex conjugate of the operator U.

Since $M^{-1} = M^{\dagger}$, we can invert the relations (II.5):

$$a_{\alpha}^{\dagger} = \sum_{\beta} \left( U_{\beta\alpha}^{*} q_{\beta}^{\dagger} + V_{\beta\alpha} q_{\beta} \right) \quad . \tag{II.9}$$

The quasiparticle vacuum is defined through the condition

$$q_{\alpha} \mid \Phi_{o} > = 0 \quad (\text{all } \alpha) \quad . \tag{II.10}$$

Thus a solution to above equation is

$$\mid \Phi_{o} > = (\text{normalization}) \cdot \prod_{\alpha} q_{\alpha} \mid 0 > \quad , \tag{II.11}$$

where $\mid 0 >$ is the particle vacuum.

Derivation of the HFB equations by the "equations-of-motion" method[8]

The density matrix $\rho$ and the pairing tensor t are defined in terms of the expectation values of the operators $a_{\beta}^{\dagger} a_{\alpha}$ and $a_{\beta} a_{\alpha}$, respectively, with respect to the quasiparticle vacuum given by equation (II.10):

$$\rho_{\alpha\beta} = < \Phi_{o} \mid a_{\beta}^{\dagger} a_{\alpha} \mid \Phi_{o} > ; \quad t_{\alpha\beta} = < \Phi_{o} \mid a_{\beta} a_{\alpha} \mid \Phi_{o} > \quad . \tag{II.12}$$

From the anticommutation relations for $a_{\alpha}^{\dagger}$s, it follows that $\rho$ is Hermitian and t is antisymmetric. One can easily evaluate $\rho$ and t by using $M^{-1}$ to convert a's into q's, in conjunction with the condition (II.10). Thus we have

$$\rho_{\alpha\beta} = \langle \Phi_o | a_\beta^\dagger a_\alpha | \Phi_o \rangle$$

$$= \langle \Phi_o | \left( \sum_\gamma U^*_{\gamma\beta} q^\dagger_\gamma + V_{\gamma\beta} q_\gamma \right) \left( \sum_\delta V^*_{\delta\alpha} q^\dagger_\delta + U_{\delta\alpha} q_\delta \right) | \Phi_o \rangle$$

$$= \sum_\gamma \sum_\delta V_{\gamma\beta} V^*_{\delta\alpha} \delta_{\gamma\delta} = \sum_\delta V_{\delta\beta} V^*_{\delta\alpha} = (V^\dagger V)_{\alpha\beta} \quad . \qquad (II.13)$$

(Here we have used the anticommutation relations

$$[q^\dagger_\alpha, q_\beta] = \delta_{\alpha\beta}, [q^\dagger_\alpha, q^\dagger_\beta] = [q_\alpha, q_\beta] = 0 ).$$

In a similar manner we can show that

$$t = V^\dagger U \quad . \qquad (II.14)$$

As a next step, we apply Wick's theorem to replace the products of operators appearing in H' by the sum of normal products containing all possible contractions (A normal product $:a_1^\dagger a_2^\dagger \ldots\ldots a_N^\dagger:$ of particle operators is obtained by first writing these operators in terms of $q^\dagger$'s and q's, and then ordering them so that the creation operators are to the left of the annihilation operators. A sign $(-1)^p$ is included where p is the number of permutations to go from the original to normal ordering sequence).

We then obtain

$$H' = H'_o + H'_2 + H'_4 \quad , \qquad (II.15)$$

where $H'_n$ involves n uncontracted operators:

$$H_o' = \mathrm{tr}\left[\left(\varepsilon - \lambda_\pi N_\pi - \lambda_\nu N_\nu + \frac{1}{2}\Gamma\right)\rho + \frac{1}{2}\Delta t^\dagger\right] , \qquad (II.16)$$

$$H_2' = \sum_{\alpha\beta}\left(h - \lambda_\pi N_\pi - \lambda_\nu N_\nu\right)_{\alpha\beta} :a_\alpha^\dagger a_\beta: + \frac{1}{2}\sum_{\alpha\beta}\Delta_{\alpha\beta} :a_\alpha^\dagger a_\beta^\dagger: + \frac{1}{2}\sum_{\alpha\beta}\Delta_{\alpha\beta}^\dagger :a_\alpha a_\beta: , \qquad (II.17)$$

$$H_4' = (1/4)\sum_{\alpha\beta\gamma\delta} \langle\alpha\beta|V_A|\gamma\delta\rangle :a_\alpha^\dagger a_\beta^\dagger a_\delta a_\gamma: . \qquad (II.18)$$

Here the HF Hamiltonian h, the HF potential $\Gamma$, and the pair potential $\Delta$ are given as

$$h = \varepsilon + \Gamma, \quad \Gamma_{\alpha\beta} = \sum_{\gamma\delta} \langle\alpha\gamma|V_A|\beta\delta\rangle \rho_{\delta\gamma} , \qquad (II.19)$$

$$\Delta_{\alpha\beta} = \frac{1}{2}\sum_{\gamma\delta}\langle\alpha\beta|V_A|\gamma\delta\rangle t_{\gamma\delta} . \qquad (II.20)$$

From the Hermiticity of $\rho$ and the antisymmetric nature of t, one can immediately deduce that $\Gamma$ is Hermitian and $\Delta$ is antisymmetric by invoking the properties of $\langle|V_A|\rangle$:

$$\langle\alpha\beta|V_A|\gamma\delta\rangle = -\langle\beta\alpha|V_A|\gamma\delta\rangle; \quad \langle\alpha\gamma|V_A|\beta\delta\rangle = \langle\beta\delta|V_A|\alpha\gamma\rangle .$$

The expectation values $\langle\Phi| :a_1^\dagger a_2^\dagger \ldots a_N^\dagger: |\Phi\rangle$ vanish by construction. Thus

$$\langle\Phi_o|H|\Phi_o\rangle = \mathrm{tr}\left[\left(\varepsilon - \lambda_\pi N_\pi - \lambda_\nu N_\nu + \frac{1}{2}\Gamma\right)\rho + \frac{1}{2}\Delta t^\dagger\right] . \qquad (II.21)$$

Now assuming an "independent quasiparticle" form for the part $H_2'$ we can write

$$H_2' = \sum_\alpha E_\alpha q_\alpha^\dagger q_\alpha . \qquad (II.22)$$

Equation (II.22) leads to the commutator

$$[\, H_2' \,,\, q_\alpha^\dagger \,] = E_\alpha q_\alpha^\dagger = E_\alpha \sum_\beta (U_{\alpha\beta} a_\beta^\dagger + V_{\alpha\beta} a_\beta) \quad . \qquad (II.23)$$

On the other hand the use of the equation (II.17) results in the expression:

$$[\, H_2', q_\alpha^\dagger] = \sum_{\beta\gamma} [\, h'_{\beta\gamma} U_{\alpha\gamma} + \Delta_{\beta\gamma} V_{\alpha\gamma}] \; a_\beta^\dagger + \sum_{\beta\gamma} [\, -\Delta^*_{\beta\gamma} U_{\alpha\gamma} - h'^*_{\beta\gamma} V_{\alpha\gamma}] a_\beta \quad . \qquad (II.24)$$

Equating the coefficients of $a_\beta^\dagger$ and $a_\beta$ we obtain the general HFB equations:

$$\begin{pmatrix} h' & \Delta \\ -\Delta^* & -h'^* \end{pmatrix} \begin{pmatrix} \vec{U}_i \\ \vec{V}_i \end{pmatrix} = E_i \begin{pmatrix} \vec{U}_i \\ \vec{V}_i \end{pmatrix} \quad , \; h' = h - \lambda_\pi N_\pi - \lambda_\nu N_\nu , \qquad (II.25)$$

where $\vec{U}_i \equiv (U_{i1}, U_{i2}, \ldots U_{iN})$.

Time-reversal Symmetry

In our calculations we have divided all the basis states in the configuration space spanned by the orbits $1f_{7/2}$, $2p_{3/2}$, $2p_{1/2}$ and $1f_{5/2}$ into two sets. The first set contains the states $|k>$, which are restricted to have $(m + 1/2)$ equal to an even integer. The second set contains the time-reversed states $|\bar{k}> = T|k>$, which have $(m + 1/2)$ = odd integer. The phase convention is $T|nljm> = (-1)^{l+j-m} |nl\; j-m>$. The first set is

$[(1f_{7/2,7/2}), (1f_{7/2,3/2}, 1f_{5/2,3/2}, 2p_{3/2,3/2}), (1f_{7/2,-1/2}, 1f_{5/2,-1/2}, 2p_{3/2,-1/2}, 2p_{1/2,-1/2})$ and $(1f_{7/2,-5/2}, 1f_{5/2,-5/2})]$

For quasiparticle operators

$$q^{\dagger}_{\alpha} = \sum_{\beta} \left( U_{\alpha\beta} a^{\dagger}_{\beta} + V_{\alpha\beta} a_{\bar{\beta}} \right) , \qquad (II.26)$$

$$q^{\dagger}_{\bar{\alpha}} = \sum_{\beta} \left( \bar{U}_{\alpha\beta} a^{\dagger}_{\bar{\beta}} + \bar{V}_{\alpha\beta} a_{\beta} \right) , \qquad (II.27)$$

we notice that $\rho$ can not connect $|k\rangle$ and $|\bar{k}\rangle$. Further the only nonzero elements of t connect the states $|k\rangle$ to the states $|\bar{k}\rangle$. Since the interaction V conserves the magnetic projections, the potentials $(\Gamma, \Delta)$ are partitioned in the same manner as the densities $(\rho, t)$.

Thus,

$$\rho = \begin{pmatrix} \rho_1 & 0 \\ 0 & \rho_2 \end{pmatrix} , \; t = \begin{pmatrix} 0 & t_1 \\ t_2 & 0 \end{pmatrix} , \; h = \begin{pmatrix} h_1 & 0 \\ 0 & h_2 \end{pmatrix} , \Delta = \begin{pmatrix} 0 & \Delta_1 \\ \Delta_2 & 0 \end{pmatrix} , \qquad (II.28)$$

where $\rho$ and h are Hermitian. Since t and $\Delta$ are by definition antisymmetric, $t_2 = -\tilde{t}_1$ and $\Delta_2 = -\tilde{\Delta}_1$.

Substitution of (II.28) into (II.25) reveals that the energy matrix is also partitioned into two blocks and that the forms (II.26), (II.27) of the wavefunctions is retained. We have imposed time-reversal symmetry by requiring that

$$q^{\dagger}_{\bar{\alpha}} = T \, q^{\dagger}_{\alpha} \, T^{-1} , \qquad (II.29)$$

so that $\bar{U}_{\alpha\beta} = U^{*}_{\alpha\beta}$, $\bar{V}_{\alpha\beta} = -V^{*}_{\alpha\beta}$. (II.30)

The quasiparticle vacuum is now time-reversal invariant and

$$\rho_2 = \rho_1^* \ , \ h_2 = h_1^* , \ t_1^\dagger = t_1 , \ \Delta_1^\dagger = \Delta_1 \ . \quad \text{(II.31)}$$

Therefore only the block of the energy matrix that is related to (II.26) is diagonalized.

Canonical representation for time-reversally symmetric HFB wavefunctions (Bloch-Messiah Theorem)

We next consider the question of simultaneous diagonalization of $\rho$ and t. We have just seen that these are Hermitian. Therefore we have to check their commutator. Consider

$$A^\dagger = \begin{pmatrix} q_\alpha^\dagger \\ q_\alpha \end{pmatrix} \ , \quad B^\dagger = \begin{pmatrix} a_\alpha^\dagger \\ a_\alpha \end{pmatrix} \ . \quad \text{(II.32)}$$

Then $$A^\dagger = M B^\dagger \ . \quad \text{(II.33)}$$

We can now define the generalized quasiparticle density matrix Q:

$$Q_{\alpha\beta} = \langle \Phi_o | A_\beta^\dagger A_\alpha | \Phi_o \rangle \ . \quad \text{(II.34)}$$

Since $\langle q_\alpha^\dagger q_\beta \rangle = \langle q_\alpha^\dagger q_\beta^\dagger \rangle = \langle q_\alpha q_\beta \rangle = 0$, $\langle q_\alpha q_\beta^\dagger \rangle = \delta_{\alpha\beta}$, we have

$$Q = \begin{pmatrix} 0 & 0 \\ 0 & 1 \end{pmatrix} \ . \quad \text{(II.35)}$$

The generalized particle density matrix is defined as

$$R_{\alpha\beta} = \langle \Phi_o | B_\beta^\dagger B_\alpha | \Phi_o \rangle \ . \quad \text{(II.36)}$$

Using the definitions (II.12) we get

$$R = \begin{bmatrix} \rho & t \\ t^\dagger & 1-\tilde{\rho} \end{bmatrix} . \qquad \text{(II.37)}$$

Inverting relation (II.33) we find that R and Q are related by a unitary transformation:

$$R = M^\dagger Q M .$$

Since $Q^2 = Q$, we have $R^2 = R$. The latter relation yields

$$\rho - \rho^2 = tt^\dagger , \qquad \text{(II.38)}$$

$$\rho t = t\tilde{\rho} . \qquad \text{(II.39)}$$

Thus $\rho_1 t_1 = t_1 \rho_1$, and this ensures that $\rho_1$ and $t_1$ can be diagonalized simultaneously. One can therefore have a basis spanned by $[|k_1\rangle, |k_2\rangle \ldots\ldots; |\bar{k}_1\rangle, |\bar{k}_2\rangle \ldots\ldots]$ such that $\rho$ and t have the canonical forms shown below:

$$\rho = \left[\begin{array}{cc|cc|c} \rho_1 & 0 & & & \\ 0 & \rho_{\bar{1}} & & & \\ \hline & & \rho_2 & 0 & \\ & & 0 & \rho_{\bar{2}} & \\ \hline & & & & \ddots \end{array}\right] , \quad t = \left[\begin{array}{cc|cc|c} 0 & t_{1\bar{1}} & & & \\ -t_{1\bar{1}} & 0 & & & \\ \hline & & 0 & t_{2\bar{2}} & \\ & & -t_{2\bar{2}} & 0 & \\ \hline & & & & \ddots \end{array}\right] . \qquad \text{(II.40)}$$

Here $|k\rangle = b_k^\dagger |0\rangle$ and

$$b_k^\dagger = \sum_\alpha C_{k,\alpha} a_\alpha^\dagger ; \quad b_{\bar{k}}^\dagger = \sum_\alpha C_{k,\alpha}^* a_{\bar{\alpha}}^\dagger . \qquad \text{(II.41)}$$

Denoting the (real) eigenvalues of Hermitian $\rho_1$ and $t_1$ by $\rho_k$ and $t_{k\bar{k}}$ respectively, we obtain from the relation (II.37)

$$| t_{k\bar{k}} | = [ \rho_k (1-\rho_k) ]^{1/2} \quad . \qquad \text{(II.42)}$$

Setting $\rho_k = V_k^2$ $(U_k^2 + V_k^2 = 1)$ we get $| t_{k\bar{k}} | = U_k V_k$ . (II.43)

Recalling the definitions (II.12) we see that the quasiparticle vacuum can be expressed as

$$| \Phi_o > = \prod_k (U_k + V_k \, b_k^\dagger \, b_{\bar{k}}^\dagger) \, | \, 0> \quad . \qquad \text{(II.44)}$$

<u>Approximations employed in the present calculations</u>

Inverting the special quasiparticle transformation

$$q_k^\dagger = U_k^* \, b_k^\dagger - V_k^* \, b_{\bar{k}} \; ; \; q_{\bar{k}}^\dagger = U_k^* \, b_{\bar{k}}^\dagger + V_k^* \, b_k \quad , \text{(II.45)}$$

and substituting in (II.17) we get

$$H_2' = H_{11}' + H_{20}' ; \; H_{11}' = \sum_{kk'} (H_{11}')_{kk'} \, q_k^\dagger \, q_{k'} \quad ;$$

$$H_{20}' = \sum_{kk'} [ (H_{20}')_{kk'} \, q_k^\dagger \, q_{k'}^\dagger + (H_{20}')^*_{kk'} \, q_{k'} \, q_k ] \, . \qquad \text{(II.46)}$$

As pointed out earlier, $H_{20}'$ acquires the form (II.22) when $H_{20}' = 0$ and $H_{11}'$ is diagonal. Whereas the condition $(H_{20}')_{k\bar{k}} = 0$ leads to the BCS equations, the requirements $(H_{20}')_{k\bar{k}} = 0$,

$(H'_{11})_{kk'} = 0$ $(k \neq k')$ lead to "HF-like" equations provided $h'_{kk'} = 0$ and $\Delta_{k\bar{k}'} = 0$ $(k \neq k')$. We have made the latter approximation, viz. $\Delta_{k\bar{k}'} = 0$. The expansion coefficients appearing in (II.41) have been obtained by diagonalizing in the spherical basis the HF-like potential $h'$ which includes the appropriate density $\rho_k = v_k^2$:

$$h'_{\alpha\beta} = \langle \alpha | \varepsilon - \lambda_\pi N_\pi - \lambda_\nu N_\nu | \beta \rangle + \sum_k \langle \alpha k | V_A | \beta k \rangle v_k^2 \quad . \qquad (II.47)$$

The occupation probabilities $v_k^2$ are obtained by solving the BCS equations:

$$\Delta_{k\bar{k}} = \sum_{k'} \langle k\bar{k} | V_A | k'\bar{k}' \rangle u_{k'} v_{k'} \quad . \qquad (II.48)$$

The calculation involves iteration between equations (II.47) and (II.48) until a reasonable convergence is achieved in terms of both the expansion coefficients $C_{k,\alpha}$ as well as the occupation probabilities $v_k^2$. Denoting by $\Theta_k$ the eigenvalues of (II.47), it turns out that the condition $(H'_{20})_{k\bar{k}} = 0$ yields

$$2\Theta_k u_k v_k - \Delta_{k\bar{k}} (u_k^2 - v_k^2) = 0 \quad . \qquad (II.49)$$

The above equation leads to the following non-trivial implicit solutions of (II.47) and (II.48) (here $u_k^2 + v_k^2 = 1$) :

$$u_k^2 = \frac{1}{2}\left[1 + \frac{\Theta_k}{\sqrt{\Theta_k^2 + \Delta_{k\bar{k}}^2}}\right], \quad v_k^2 = \frac{1}{2}\left[1 - \frac{\Theta_k}{\sqrt{\Theta_k^2 + \Delta_{k\bar{k}}^2}}\right] \quad . \qquad (II.50)$$

Using (II.50) in (II.48) one gets

$$\Delta_{k\bar{k}} = \frac{1}{2} \sum_{k'} \langle k\bar{k}|V_A|k'\bar{k}'\rangle \frac{\Delta_{k'\bar{k}'}}{\sqrt{\theta_{k'}^2 + \Delta_{k'\bar{k}'}^2}} \quad . \qquad (II.51)$$

The condition $2 \sum_{k} V_{k,\pi/\nu}^2 = N_{\pi/\nu}$ yields

$$\sum_{\substack{k \\ \pi/\nu}} \left[1 - \frac{\theta_k}{\sqrt{\theta_k^2 + \Delta_{k\bar{k}}^2}}\right] = N_{\pi/\nu} \quad . \qquad (II.52)$$

## II.2.2 Calculation of Subshell Occupation Numbers in Terms of States of Good Angular Momentum Projected from the HFB Intrinsic States

Restricting ourselves to axially symmetric states $|\Phi_o\rangle$, we can label the states $|k\rangle$ by the expectation values of the operator $\hat{J}_z$. Thus the axially symmetric intrinsic deformed HFB states with $K = 0$ given by equation (II.44) can be written as

$$|\Phi_o\rangle = \prod_{im} (U_i^m + V_i^m b_{im}^\dagger b_{i\bar{m}}^\dagger)|0\rangle \quad , \qquad (II.53)$$

where the creation operators $b_{im}^\dagger$ can be expressed as

$$b_{im}^\dagger = \sum_j C_{ji}^m a_{jm}^\dagger ; \; b_{i\bar{m}}^\dagger = \sum_j (-1)^{j-m} C_{ji}^m a_{j-m}^\dagger . \qquad (II.54)$$

Here, the index i is used to distinguish between different states with the same m, and j labels the spherical single particle orbitals $1f_{7/2}$, $2p_{3/2}$, $2p_{1/2}$ and $1f_{5/2}$. The wave function expressed in eqn.(II.53) can be recast into the form[12]

$$| \Phi_o > = N \exp \left( \frac{1}{2} \sum_{\alpha\beta} f_{\alpha\beta} a^\dagger_\alpha a^\dagger_\beta \right) | 0 > , \qquad (II.55)$$

with

$$f_{\alpha\beta} = \sum_i C^{m_\alpha}_{j_\alpha i} C^{m_\beta}_{j_\beta i} \frac{v^{m_\alpha}_i}{U^{m_\alpha}_i} \delta_{m_\alpha, -m_\beta} . \qquad (II.56)$$

Here we have denoted the quantum numbers $(j_\alpha, m_\alpha)$ by $\alpha$, and N is a normalisation constant.

The states with good angular momenta J projected from the HFB state $| \Phi_K >$ can be written as

$$| \Psi^J_K > = P^J_{KK} | \Phi_K > = \left( \frac{2J+1}{8\pi^2} \right) \int D^J_{KK}(\Omega) \, R(\Omega) \, | \Phi_K > d\Omega , \qquad (II.57)$$

where $R(\Omega)$ and $D^J_{KK}(\Omega)$ are the rotation operator and the rotation matrix respectively.

In terms of the angular momentum projected states $|\Psi^J_K>$ the expectation value of the operator $\hat{\eta}_j$:

$$\hat{\eta}_j = \sum_{m=-j}^{+j} a^\dagger_{jm} a_{jm} \qquad (II.58)$$

can be expressed as

$$\begin{aligned} \eta_j &= < \Psi^J_K | \hat{\eta}_j | \Psi^J_K > \\ &= <\Phi_o | \left( \sum_{m=-j}^{+j} a^\dagger_{jm} a_{jm} \right) P^J_{oo} | \Phi_o > / <\Phi_o | P^J_{oo} | \Phi_o > \\ &= \int_o^\pi p(\theta) \, d^J_{oo}(\theta) \sin\theta \, d\theta / \int_o^\pi n(\theta) d^J_{oo}(\theta) \sin\theta \, d\theta , \end{aligned} \qquad (II.59)$$

where

$$p(\Theta) = n(\Theta) \left[ \sum_{m=-j}^{+j} \rho_{jm;jm} \right] . \qquad (II.60)$$

The density matrix $\rho(\Theta)$ is defined as

$$\rho(\Theta) = \frac{M(\Theta)}{1+M(\Theta)} . \qquad (II.61)$$

Here $$M(\Theta) = F(\Theta) \; f^{\dagger} \qquad (II.62)$$

and $$F_{\alpha\beta}(\Theta) = \sum_{m'_\alpha m'_\beta} d^{j_\alpha}_{m_\alpha m'_\beta}(\Theta) \; d^{j_\beta}_{m_\beta m'_\beta}(\Theta) \; f_{j_\alpha m'_\alpha , j_\beta m'_\beta} . \qquad (II.63)$$

Further we have

$$n(\Theta) = \sqrt{\det (1+M(\Theta))} . \qquad (II.64)$$

The subshell occupation numbers were calculated as follows. The results of the variational HFB calculation are summarized in terms of the amplitudes ($U_i^m$, $V_i^m$) and the expansion coefficients $C^m_{ji}$. These values are used to first set up the f matrix. We next evaluate F, M and 1/(1+M) for 20 values of the Gaussian quadrature points lying in the range $(0,\pi/2)$. Finally, the subshell occupation numbers for the ground state are computed from equation (II.59).

It should be mentioned here that an approximate expression of the subshell occupation numbers can easily be obtained in terms of the expectation value of the operator $\hat{\eta}_j$ with respect to the intrinsic state $|\Phi_o\rangle$,

$$\eta_j \sim \langle \Phi_o | \hat{\eta}_j | \Phi_o \rangle = \sum_{im} |C^m_{ji}|^2 (V^m_i)^2 . \qquad (II.65)$$

The expression (II.65) has in fact earlier[13] been employed for

calculating subshell occupation numbers in some doubly even Ni isotopes. It should however be emphasized that the estimates obtained from equation (II.65) provide the values averaged over the complete yrast band consisting of the states with J=0 to $J = J_{max}$ ($\sim 16\hbar$). These 'band-averaged' values are likely to differ significantly from the estimates based on the use of the projected J=0 wave functions given by Eq.(II.59). This is because the considerations of angular momentum coupling require enhanced involvement of high-j subshells in the structure of high spin members of the yrast band.

## II.3 Results and Discussion

In our calculations we have employed the Kuo-Brown[14] (KB) effective interaction for the ($1f_{7/2}$, $2p_{3/2}$, $2p_{1/2}$, $1f_{5/2}$) valence space as well as a slightly modified version of the KB interaction suggested by McGrory, Wildenthal and Halbert[15] (MWH). The KB interaction consists of the bare interaction derived from the empirical Hamada-Johnston potential and the renormalisation due to the three-particle one-hole (3p-1h) excitation in the $^{40}$Ca core (see Appendix A). McGrory et al.[15] later found it necessary to modify the T = 1 part of the KB interaction with a view to optimize the agreement between the shell model and the experimental spectra for some calcium isotopes. The modified version of the KB interaction is hereafter labelled as the MWH interaction. The set of single-particle energies we have taken are (in MeV): $\varepsilon(1f_{7/2}) = 0.0$,

$\varepsilon(2p_{3/2}) = 2.1$, $\varepsilon(2p_{1/2}) = 3.9$ and $\varepsilon(1f_{5/2}) = 6.5$.

II.3.1 Comparison of the observed subshell occupation numbers with the predictions resulting from the KB and the MWH interactions in the framework of the HFB method involving explicit angular momentum projection

The results for the subshell occupation numbers for the $1f_{7/2}$, $2p_{3/2}$, $2p_{1/2}$ and $1f_{5/2}$ orbits obtained via the PHFB method for various Ti, Cr, Fe, Ni, Zn and Ge isotopes are given in Figure II.1. The solid (dashed) straight lines join the theoretical estimates obtained with the MWH (KB) interaction. The experimental information about the spectroscopic factors for various pick-up and stripping reactions is given in reference 1 for Ti isotopes, reference 2 for Cr isotopes, reference 3 for $^{56}$Fe, reference 4 for Ni isotopes, reference 5 for Zn isotopes and reference 6 for $^{70}$Ge. The experimental values for the sub-shell occupation numbers shown here (filled circles) were extracted from the available spectroscopic factors by Kota and Potbhare[9] using the non-energy-weighted French-MacFarlane sum rules[7].

An examination of the results presented in Table II.1 and Figure II.1 reveals the following:

(1) The results obtained from the interactions KB and MWH differ significantly in terms of the predictions concerning the $(\frac{7}{2})_{\pi,\nu}$ orbit in the nuclei $^{50,52,54}$Cr, $^{54,56}$Fe and $^{56,58}$Ni. In the nucleus $^{56}$Ni, for example, the subshell

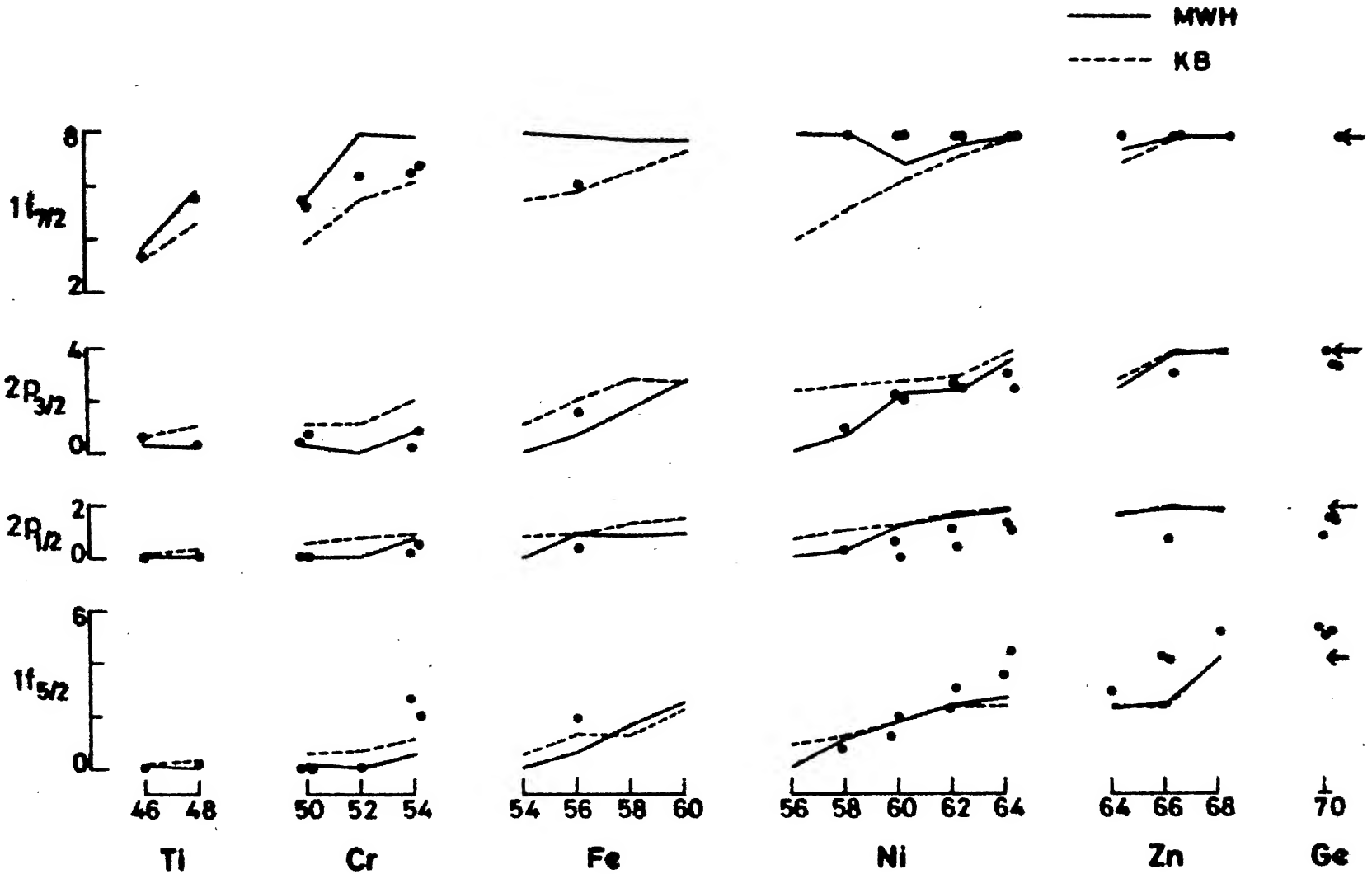


FIG. II.1 COMPARISON OF THE OBSERVED SUBSHELL OCCUPATION NUMBERS WITH THE THEORETICAL ESTIMATES.

TABLE II.1

The sub-shell occupation numbers for protons and neutrons resulting from the KB and the MWH interactions are tabulated. The nature of the minimum-energy HFB solution—prolate (P), oblate (O) and spherical (S) — is also indicated. The intrinsic quadrupole moments have been given in units of $b^2$, where b is the oscillator parameter.

| Nucleus | Interaction | $Q_{HFB}$ (Type of HFB minimum) | Subshell Occupation Numbers | | | | | | | |
|---|---|---|---|---|---|---|---|---|---|---|
| | | | Protons | | | | Neutrons | | | |
| | | | $j = \frac{7}{2}$ | $\frac{5}{2}$ | $\frac{3}{2}$ | $\frac{1}{2}$ | $\frac{7}{2}$ | $\frac{5}{2}$ | $\frac{3}{2}$ | $\frac{1}{2}$ |
| $^{46}Ti$ | MWH | 22.57 (P) | 1.58 | 0.03 | 0.34 | 0.05 | 3.57 | 0.11 | 0.28 | 0.04 |
| | KB | 24.98 (P) | 1.36 | 0.04 | 0.53 | 0.09 | 3.24 | 0.15 | 0.53 | 0.08 |
| $^{48}Ti$ | MWH | 16.43 (P) | 1.71 | 0.03 | 0.14 | 0.01 | 5.78 | 0.08 | 0.18 | 0.03 |
| | KB | 25.51 (P) | 1.31 | 0.03 | 0.57 | 0.07 | 4.53 | 0.24 | 1.01 | 0.28 |
| $^{50}Cr$ | MWH | 25.51 (P) | 3.66 | 0.07 | 0.26 | 0.01 | 5.49 | 0.15 | 0.29 | 0.06 |
| | KB | 35.46 (P) | 2.96 | 0.18 | 0.80 | 0.08 | 3.94 | 0.49 | 1.02 | 0.54 |
| $^{52}Cr$ | MWH | -2.53 (O) | 3.88 | 0.08 | 0.02 | 0.02 | 8.00 | 0.00 | 0.00 | 0.00 |
| | KB | 37.11 (P) | 2.91 | 0.15 | 0.88 | 0.08 | 5.54 | 0.61 | 1.09 | 0.77 |
| $^{54}Cr$ | MWH | 26.73 (P) | 3.63 | 0.08 | 0.30 | 0.02 | 7.87 | 0.57 | 0.81 | 0.76 |
| | KB | 33.86 (P) | 2.96 | 0.12 | 0.86 | 0.06 | 6.20 | 1.04 | 2.01 | 0.86 |
| $^{54}Fe$ | MWH | -1.27 (O) | 5.90 | 0.07 | 0.02 | 0.01 | 8.00 | 0.00 | 0.00 | 0.00 |
| | KB | 41.15 (P) | 3.75 | 0.40 | 1.20 | 0.62 | 5.46 | 0.52 | 1.19 | 0.83 |
| $^{56}Fe$ | MWH | 25.52 (P) | 5.72 | 0.07 | 0.20 | 0.01 | 7.88 | 0.58 | 0.68 | 0.85 |
| | KB | 39.74 (P) | 3.84 | 0.25 | 1.30 | 0.58 | 5.79 | 1.34 | 2.01 | 0.89 |
| $^{58}Fe$ | MWH | 26.73 (P) | 5.71 | 0.08 | 0.21 | 0.00 | 7.76 | 1.62 | 1.78 | 0.81 |
| | KB | -33.05 (O) | 3.51 | 0.23 | 1.70 | 0.30 | 6.74 | 1.23 | 2.80 | 1.28 |
| $^{60}Fe$ | MWH | 26.19 (P) | 5.68 | 0.08 | 0.24 | 0.00 | 7.84 | 2.46 | 2.81 | 0.93 |
| | KB | -33.72 (O) | 3.89 | 0.23 | 1.51 | 0.21 | 7.50 | 2.23 | 2.71 | 1.56 |

Continued.....

TABLE II.1( Continued):

| Nucleus | Interaction | $Q_{HFB}$ (Type of HFB minimum) | Subshell Occupation Numbers | | | | | | | |
|---|---|---|---|---|---|---|---|---|---|---|
| | | | Protons | | | | Neutrons | | | |
| | | | $j = \frac{7}{2}$ | $\frac{5}{2}$ | $\frac{3}{2}$ | $\frac{1}{2}$ | $\frac{7}{2}$ | $\frac{5}{2}$ | $\frac{3}{2}$ | $\frac{1}{2}$ |
| $^{56}$Ni | MWH | 0.00 (S) | 8.00 | 0.00 | 0.00 | 0.00 | 8.00 | 0.00 | 0.00 | 0.00 |
| | KB | -44.16 (O) | 4.00 | 0.82 | 2.42 | 0.76 | 4.00 | 0.82 | 2.42 | 0.76 |
| $^{58}$Ni | MWH | - 3.54 (O) | 8.00 | 0.00 | 0.00 | 0.00 | 7.90 | 1.10 | 0.72 | 0.28 |
| | KB | -41.98 (O) | 4.15 | 0.64 | 2.50 | 0.71 | 5.29 | 1.14 | 2.58 | 1.07 |
| $^{60}$Ni | MWH | -38.03 (O) | 5.31 | 0.33 | 1.93 | 0.43 | 6.83 | 1.63 | 2.34 | 1.23 |
| | KB | -40.51 (O) | 4.35 | 0.46 | 2.56 | 0.63 | 6.35 | 1.66 | 2.71 | 1.31 |
| $^{62}$Ni | MWH | -37.76 (O) | 5.71 | 0.21 | 1.82 | 0.25 | 7.65 | 2.33 | 2.36 | 1.65 |
| | KB | -40.09 (O) | 4.55 | 0.32 | 2.64 | 0.49 | 7.33 | 2.31 | 2.67 | 1.69 |
| $^{64}$Ni | MWH | -24.39 (O) | 7.07 | 0.07 | 0.83 | 0.03 | 7.94 | 2.70 | 3.71 | 1.77 |
| | KB | -29.41 (O) | 4.77 | 0.22 | 2.66 | 0.35 | 7.94 | 2.31 | 3.90 | 1.84 |
| $^{64}$Zn | MWH | -36.92 (O) | 6.42 | 0.42 | 2.33 | 0.83 | 7.60 | 2.24 | 2.44 | 1.72 |
| | KB | -38.21 (O) | 5.66 | 0.55 | 2.81 | 0.96 | 7.12 | 2.34 | 2.85 | 1.68 |
| $^{66}$Zn | MWH | -24.92 (O) | 6.94 | 0.19 | 2.16 | 0.71 | 7.93 | 2.41 | 3.83 | 1.85 |
| | KB | -26.09 (O) | 5.94 | 0.26 | 2.97 | 0.88 | 7.94 | 2.25 | 3.92 | 1.89 |
| $^{68}$Zn | MWH | -17.42 (O) | 7.72 | 0.01 | 1.70 | 0.36 | 8.00 | 4.06 | 4.01 | 1.93 |
| | KB | -20.01 (O) | 6.70 | 0.13 | 2.75 | 0.42 | 7.99 | 4.15 | 3.98 | 1.87 |
| $^{70}$Ge | MWH | -18.60 (O) | 7.95 | 0.02 | 3.31 | 0.72 | 8.00 | 4.05 | 4.01 | 1.94 |
| | KB | -17.50 (O) | 7.65 | 0.01 | 3.40 | 0.94 | 7.99 | 4.12 | 3.97 | 1.92 |

occupation numbers coming from KB and MWH interactions differ by four particles. In the case of the nuclei $^{56,58}$Ni even the predictions for the orbit $p_{3/2}$ differ by more than one particle.

(2) It is seen that both the interactions KB and MWH predict identical results for the various orbits in cases of all the nuclei with A $\geq$ 60. This convergence of the occupation numbers for the two interactions in the second half of the 2p-1f shell is related to the fact that these interactions differ primarily in terms of the relative positions of the centroids of the interactions operative in the $(\frac{7}{2}\ \frac{7}{2})$ and $(\frac{7}{2}\ \frac{3}{2})$ configurations. The relative importance of the orbits $\frac{7}{2}$ and $\frac{3}{2}$, however, decreases for the nuclei with A $\geq$ 60 considered here.

(3) In the nuclei $^{46,48}$Ti, $^{50}$Cr and $^{58}$Ni the predictions resulting from the MWH interaction are in distinctly better agreement with the experiments than those resulting from the KB interaction. In the nuclei $^{60,62,64}$Ni and $^{70}$Ge the predictions of both the KB as well as the MWH interactions are in reasonably good agreements with the experiments. In the nucleus $^{56}$Fe, however, the predictions resulting from the KB interaction for the various orbits separately, are in better agreement with the experiments compared to those resulting from the MWH interaction. This apparent superiority of the KB interaction is, however, not sustained if one considers

the total strength for the l = 1 and l = 3 transfers. For example, the predictions of the KB interaction, viz. the values 2.90 and 7.13 for l = 1 and l = 3 respectively, differ significantly from the experimental values which are 1.93 and 8.07 respectively. The MWH interaction on the other hand predicts values 1.54 and 8.46 which are within 20% of the experimental values. Interestingly enough, although it appears difficult at first sight to judge in favour of either of the two interactions in terms of their predictions for subshell occupation numbers for individual orbits in the case of the nucleus $^{54}Cr$, a consideration of the total strength of the l-transfers again brings out the superority of the MWH interaction.

(4) A comparison of the theoretical occupancy estimates for the orbits $2p_{3/2}$, $2p_{1/2}$ and $1f_{5/2}$ resulting from the KB and the MWH interactions with the observed ones reveals a slight underestimation of the involvement of the $f_{5/2}$ orbits. This may be implying the necessity of further modification of the part of the effective interaction MWH operating in the upper half of the $2p_{3/2}$, $2p_{1/2}$ and $1f_{5/2}$ space. However, it is seen that the observed quantitative variation of the subshell occupation number associated with the orbits $2p_{3/2}$, $2p_{1/2}$ and $1f_{5/2}$ as a function of the neutron number is reproduced reasonably well by the MWH interaction.

## II.3.2 Comparative study of the spectral distribution as well as the projected HFB methods

In this section we compare the PHFB predictions with the estimates resulting from the spectral distribution method. The calculations are carried out with the KB as well as the MWH effective interactions. These calculations are intended to assess the relative efficacy of the two methods to bring out the differences in the two interactions in terms of their predictions for the occupation numbers. In Figure II.2 we present our results for the orbits $1f_{7/2}$ and $2p_{3/2}$. A comparison of the results obtained by the MWH interaction with those resulting from the KB interaction brings out the relative insensitivity of the spectral distribution method towards the shell closure properties of the interaction. Compared to the KB interaction the interaction MWH involves enhanced attraction in the $(f_{7/2})^2$ states and an additional repulsion for the $(f_{7/2}\ p_{3/2})$ states. Consequently, the interaction MWH is expected to yield a near closure of the $f_{7/2}$-shell for nuclei with N and/or Z = 28. The PHFB calculation successfully reflects this feature; the PHFB estimates for subshell occupation resulting from the two interactions in the nuclei $^{52}Cr$ and $^{54}Fe$ display large differences. Although, the spectral distribution estimates are qualitatively consistent with the PHFB ones, one finds that the effects due to the subshell closure are significantly scaled down. It is not particularly surprising, since the involvement of a large number of single

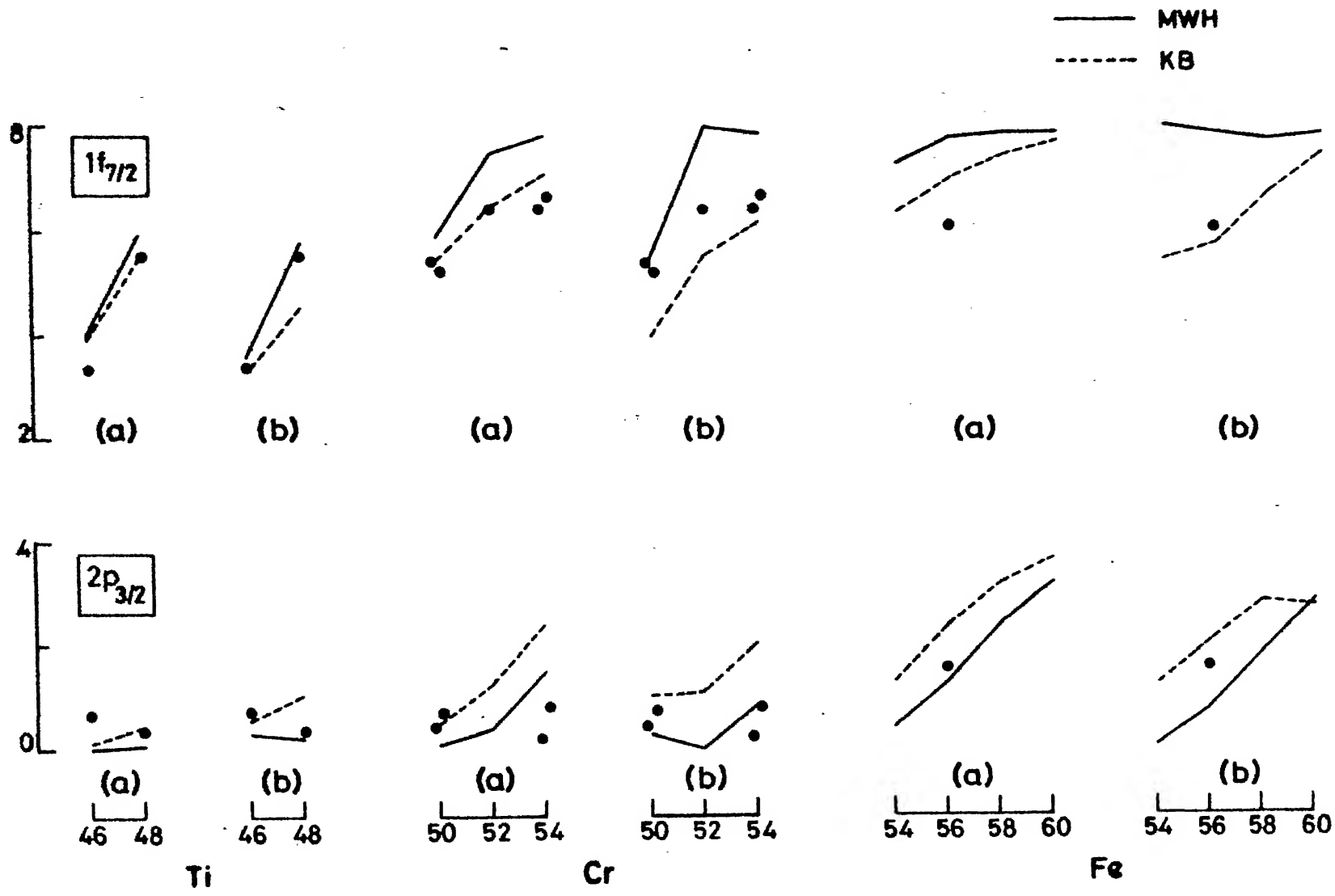


FIG. II.2 THE SUBSHELL OCCUPATION NUMBERS RESULTING FROM (a) THE SPECTRAL DISTRIBUTION METHOD AND (b) THE PHFB METHOD.

particle states — a feature which excludes sub-shell closures — is an essential prerequisite for the applicability of the spectral distribution method involving just the first two moments of the eigenvalue distribution.

## II.4 Conclusions

A simple way to examine the suitability of various effective interactions from the point of view of detailed spectroscopic calculations is to compare the ground state occupation numbers generated from those interactions with the available experimental values. However, in view of the intractability of the exact shell-model calculations in the 2p-1f shell it is worthwhile to employ simple yet reliable methods — such as the HFB method involving angular momentum projection — for the calculation of the ground state occupation numbers.

From the results presented here it turns out that the MWH interaction provides a consistently good overall description of the available subshell occupation data in a majority of the nuclei considered here. The results presented here also indicate that the spectral distribution method is not sensitive enough to permit a comparative study of two effective interactions via only their occupancy estimates in cases where sub-shell closures are involved.

## REFERENCES


1. M.L. Halbert, Nucl. Data Sheets 22, 59 (1977).

2. A.E. MacGregor and G. Brown, Nucl. Phys. A190, 548 (1972); J.E. Robertshaw, S. Mecca, A. Sperduto and W.W. Buechner, Phys. Rev. 170, 1013 (1968); R.L. Auble, Nucl. Data Sheets 21, 323 (1977); M.S. Chowdhury, A.R. Majumdar and H.M. Sen Gupta, Nucl. Phys. A282, 87 (1977).

3. R.L. Auble, Nucl. Data Sheets 20, 253 (1977).

4. R.H. Fulmer and W.W. Daehnick, Phys. Rev. 139, B579 (1965); R.H. Fulmer, A.L. McCarthy, B.L. Cohen and R. Middleton, Phys. Rev. 133, B955 (1964).

5. E.K. Lin and B.L. Cohen, Phys. Rev. 132, 2632 (1963); D. von Ehrenstein and J.P. Schiffer, Phys. Rev. 164, 1374 (1967); A.L. Abu-Ghazaleh, I.M. Naqib and G. Brown, J. Phys. G 3, 253 (1977).

6. K.R. Alvar, Nucl. Data Sheets 10, 205 (1973); J.A. Bieszk, Luis Montestruque and S.E. Darden, Phys. Rev. C16, 1333 (1977); W.A. Yoh, S.E. Darden and S. Sen, Nucl. Phys. A263, 419 (1976).

7. J.B. French and M.H. MacFarlane, Nucl. Phys. 26, 168 (1961); J.P. Schiffer, in Isospin in Nuclear Physics, edited by D.H. Wilkinson (North-Holland, Amsterdam, 1969), p. 665.

8. A.L. Goodman, in Advances in Nuclear Physics, edited by J.W. Negele and E. Vogt (Plenum, New York, 1979), Vol. 11.

9. V.K.B. Kota and V. Potbhare, Nucl. Phys. A331, 93 (1979).

10. J.B. French, Proceedings of International School of Physics "Enrico Fermi", Course 36, edited by C. Bloch (Academic, New York, 1966), p. 278.

11. F.S. Chang, J.B. French and T.H. Thio, Ann. of Phys.(NY) 66, 137 (1971).

12. N. Onishi and S. Yoshida, Nucl. Phys. 80, 367 (1966); S.K. Sharma, Nucl. Phys. A260, 226 (1976).

13. S.K. Sharma, Phys. Lett. 49B, 5 (1974).

14. T.T.S Kuo and G.E. Brown, Nucl. Phys. A114, 241 (1968).

15. J.B. McGrory, B.H. Wildenthal, and E.C. Halbert, Phys. Rev. C2, 186 (1970).

# CHAPTER III

## INELASTIC ELECTRON SCATTERING FORM FACTORS FOR THE EXCITATION OF THE YRAST $2^+$ STATES IN SOME 2p-1f SHELL NUCLEI

### III.1 Introduction

In this Chapter we present the calculation of the Coulomb form factors for the $0^+ \rightarrow 2_1^+$ transitions in the doubly even nuclei $^{46,48,50}Ti$, $^{50,52}Cr$ and $^{54,56}Fe$. Apart from the Coulomb form factors we shall also discuss here the results of the calculations of the static quadrupole moments, $Q_{2^+}$, for the $2_1^+$ states, and the reduced transition probabilities for E2 transitions, $B(E2; 0^+ \rightarrow 2_1^+)$, in these nuclei.

Inelastic electron scattering provides a powerful method for investigating nuclear structure.[1,2] This is because the momentum-transfer dependence of the nuclear matrix elements contains information about the spatial structure of the ground and the excited states, in comparison with the ordinary gamma transitions. The calculations presented here demonstrate how the available form factor data can serve to characterize the essential structural differences in various nuclei in the A = 40-60 region.

Recent years have witnessed a significant increase in the experimental data on the $0^+ \rightarrow 2_1^+$ transitions in the 2p-1f shell nuclei[3-7]. Within a measured momentum-transfer

range upto $q_{eff} \sim 2.0$ fm$^{-1}$, the C2 form factors are characterized by two peaks appearing at $q_{eff} \sim 0.7$ fm$^{-1}$ as well as at $q_{eff} \sim 1.7$ fm$^{-1}$. The magnitudes of these peaks are expected to provide a sensitive test of nuclear models.

In a recent shell-model study by Iwamoto et al[7]., the C2 form factors for some Ti, Cr and Fe isotopes were calculated in terms of wave functions resulting from empirical effective interactions operating in restricted valence space involving the $f_{7/2}^{n} + f_{7/2}^{n-1} p_{3/2}$ configurations. Their calculations, which involved proton and neutron effective charges possessing relatively strong number dependence, showed that the systematic deficiencies of the $f_{7/2}^{n}$ model, vis-à-vis the relative magnitudes of form factors at the two peaks, can be partially remedied by the $f_{7/2}^{n} + f_{7/2}^{n-1} p_{3/2}$ model. In this Chapter we show that the projected Hartree-Fock-Bogoliubov (PHFB) wave functions resulting from appropriate realistic effective interactions operating in full 2p-1f shell permit a consistent microscopic description of the available data on C2 form factors in terms of nearly constant effective charges.

In Section III.2 we discuss some details of the calculational frame work. Section III.3 discusses the comparison of the calculated Coulomb form factors and E2 transition strengths involving the $0^+$ and $2_1^+$ levels, as well as the static quadrupole moments for the $2_1^+$ states with the available experimental results. Section III.4

contains some concluding remarks.

## III.2 Calculational Framework

### III.2.1 Inelastic Scattering to Discrete Nuclear Levels

In this section we present an outline[2] of the basic formalism relevant for a discussion of the electro-excitation of nuclear levels.

We consider the inelastic electron scattering in the one-photon-exchange approximation. Let an incident electron with four-momentum $k_{1\mu} = (\vec{k}_1, iE_1)$ be scattered through an angle $\Theta$ to the four-momentum $k_{2\mu} = (\vec{k}_2, iE_2)$. The process involves the exchange of a virtual photon with four-momentum $q = (\vec{q}, iE)$. For electron energies of interest (hundreds of MeV's) we can take $E_1 \simeq k_1$ and $E_2 \simeq k_2$. The process of inelastic scattering satisfies the kinematic equations

$$\vec{k}_1 - \vec{k}_2 = \vec{q} \; ; \quad q = (k_1^2 + k_2^2 - 2k_1k_2\cos\Theta)^{1/2} \; ; \qquad \text{(III.1)}$$

$$k_1 + M = k_2 + E' \; , \qquad \text{(III.2)}$$

with

$$E' = (q^2 + M'^2)^{1/2} \; . \qquad \text{(III.3)}$$

Here M and M' are the target masses before and after excitation, respectively.

The Hamiltonian describing the interaction of the nucleus with the electromagnetic field $(\vec{A}, i\Phi_e)$ of the

electron is

$$H = H_C + H_T \quad , \qquad \text{(III.4)}$$

where the Coulomb part is

$$H_C = e \int \rho_N(\vec{r})\ \Phi_e(\vec{r})\ d^3r \qquad \text{(III.5)}$$

and the transverse part is

$$H_T = -e \int [\vec{j}_c(\vec{r}).\ \vec{A}(\vec{r}) + \vec{\mu}_s(\vec{r}).\vec{\nabla}x\ \vec{A}(\vec{r})]\ d^3r \ . \qquad \text{(III.6)}$$

Here $e\rho_N(\vec{r})$ is the nuclear charge density (with $\int \rho(\vec{r}) d^3r = Z$), $e\ \vec{j}_c(\vec{r})$ is the nuclear current density and $e\vec{\mu}_s(\vec{r})$ is the nuclear magnetization density. (The actual form of appropriate quantum mechanical operators relevant for the inelastic scattering will be given a little later in this section).

From now onwards we consider only the Coulomb interaction. Writing $\Phi_e(\vec{r})$ as

$$\Phi_e(\vec{r}) = \int [\rho_e(\vec{r}')/|\vec{r} - \vec{r}'|] d^3r' \quad , \qquad \text{(III.7)}$$

we obtain

$$H_C = e \int [\rho_N(\vec{r})\ \rho_e(\vec{r}')/|\vec{r} - \vec{r}'|]\ d^3r\ d^3r' \ . \qquad \text{(III.8)}$$

Expressing $R^{-1}$ $(R = |\vec{r} - \vec{r}'|)$ as

$$(1/R) = (2\pi)^{-3} \int \exp(i\vec{q}.\vec{R}) [e^{-i\vec{q}.\vec{R}'}/R']\ d^3R'\ d^3q$$

and evaluating the integral w.r.t. R' we get

$$|\vec{r} - \vec{r}'|^{-1} = (2\pi^2)^{-1} \int \exp[i\vec{q}.(\vec{r} - \vec{r}')]\, q^{-2}\, d^3q \quad . \quad (III.9)$$

Using this equation in conjunction with the multipole expansion of a plane wave viz.

$$\exp(i\,\vec{q}.\vec{r}) = 4\pi \sum_{LM} i^L\, j_L(qr)\, Y^*_{LM}(\hat{q})\, Y_{LM}(\hat{r}) \quad ,$$

we can rewrite equation (III.8) as

$$H_C = (2e/\pi) \sum_{LM} \int (d^3q/q^2)\, Y^*_{LM}(\hat{q})\, f_{LM}(q)\, X(\vec{q}) \quad . \quad (III.10)$$

Here $X(\vec{q})$ denotes the Fourier transform of the electron cnarge density $\rho_e(\vec{r})$:

$$X(\vec{q}) = \int \rho_e(\vec{r}\,')\, \exp(-i\vec{q}.\vec{r}')\, d^3r' \qquad (III.11)$$

and $f_{LM}(q)$ is the nuclear matrix element

$$f_{LM}(q) = i^L \int \rho_N(\vec{r})\; j_L(qr)\, Y_{LM}(\hat{r})\, d^3r \quad . \quad (III.12)$$

Putting in plane waves to lowest order for the incident and outgoing electrons,

$$\Psi_i = u(\vec{k}_1)\, \exp\, i(\vec{k}_1.\vec{r} - \omega t), \quad \Psi_f = u(\vec{k}_2)\, \exp\, i(\vec{k}_2.\vec{r} - \omega t), \qquad (III.13)$$

and employing the expression $\rho_e = -e\,\bar{\Psi}_f\, \gamma_4\, \Psi_i$ for the transition charge density, we can simplify the expression (III.11):

$$\begin{aligned} X(\vec{q}) &= -e \int \bar{u}(\vec{k}_2)\, \exp\, i(-\vec{k}_2.\vec{r}' + \omega t)\, \gamma_4\, \exp i(\vec{k}_1.\vec{r}' - \omega t)\, u(\vec{k}_1) \\ &\qquad \exp\,(-i\,\vec{q}.\vec{r}')\, d^3r' \\ &= -e\,(2\pi)^3\, \delta(\vec{k}_1 - \vec{k}_2 - \vec{q})\; (\bar{u}(\vec{k}_2)\, \gamma_4\, u(\vec{k}_1)) \quad . \quad (III.14) \end{aligned}$$

From equation (III.10) we then obtain

$$H_C = -(16\pi^2 e/q^2)\ (\bar{u}(\vec{k}_2)\ \gamma_4 u(\vec{k}_1))\ \sum_{LM} Y^*_{LM}(\hat{q})\ f_{LM}(q)\ . \qquad (III.15)$$

In the framework of the one-photon exchange approximation, the differential cross section is next obtained by multiplying $|H_C|^2$ by $2\pi$ times the appropriate phase space. The latter is given by

$$(2\pi)^{-3}\ d^3k_2\ \delta(k_1 + M - k_2 - E')\ ;\ (\Omega = 1)\ . \qquad (III.16)$$

As pointed out by Überall[2], the dynamic (nuclear) recoil effects, involving the free motion of the nuclear centre of mass, do not affect at all this phase-space factor which summarizes just the kinematic recoil effects. The cross section in the laboratory frame is thus

$$d\sigma = (2\pi E_1/k_1)\ \delta(k_1+M-k_2-E')(m_e^2/E_1E_2)\ |H_C|^2\ d^3k_2/(2\pi)^3\ . \qquad (III.17)$$

Here the factor $(m_e^2/E_1E_2)$ is due to the invariant normalization of the spinors $u(\vec{k}_{1,2})$ and $(k_1/E_1)$ is just the incident electron flux.

Considering the scattering of the outgoing electron into the solid angle $d\Omega$ we obtain

$$\int \delta(k_1+M-k_2-E'(k_2))\, d^3k_2 = k_2^2\, d\Omega\, |1+dE'(k_2)/dk_2|^{-1}$$

$$= k_2^2\, d\Omega\,[1+(2k_1/M)\sin^2(\theta/2)]^{-1}, \qquad \text{(III.18)}$$

since we have $dE'(k_2)/dk_2 = (dE'/dq)\,(dq/dk_2)$

$$= (q/E')\,(dq/dk_2), \qquad \text{(III.19)}$$

using the equations (III.3) and (III.1) and employing the approximations $E' \cong M$, $k_2 = k_1$.

The term $|H_C|^2$ in equation (III.17) involves the expression $|\bar{u}(\vec{k}_2)\,\gamma_4\,u(\vec{k}_1)|^2$. The actual cross section involves a sum of this expression over final spin states and an average over initial states; it should therefore be replaced by

$$\frac{1}{2} \sum_{s_f, s_i} |\bar{u}(\vec{k}_2, s_f)\,\gamma_4\,u(\vec{k}_1, s_i)|^2 . \qquad \text{(III.20)}$$

The spin sum can be rewritten as

$$\sum_{s_f, s_i} \bar{u}_\alpha(\vec{k}_2, s_f)\,(\gamma_4)_{\alpha\beta}\,u_\beta(\vec{k}_1, s_i)\;\bar{u}_\delta(\vec{k}_1, s_i)(\gamma_4)_{\delta\sigma}\,u_\sigma(\vec{k}_2, s_f) . \qquad \text{(III.21)}$$

It can be shown that[8]

$$\sum_{s_i} u_\beta(\vec{k}_1, s_i)\;\bar{u}_\delta(\vec{k}_1, s_i) = [(\not{k}_1 + im_e)/2im_e]_{\beta\delta}.$$

Thus the expression (III.21) simplifies to

$$\mathrm{Tr}\,[((\not K_2+im_e)/2im_e)\,\gamma_4((\not K_1+im_e)/2im_e)\gamma_4]$$

$$= (E_1E_2 + \vec{k}_1.\vec{k}_2 + m_e^2)/m_e^2 \ . \qquad \text{(III.22)}$$

We next replace the nuclear matrix element $f_{LM}(q)$ by its operator definition, viz.

$$f_{LM}^{op}(q) = i^L \int \rho^{op}(\vec{r})\ j_L(qr)\ Y_{LM}(\hat{r})\ d^3r$$

$$= i^L \sum_k e_k j_L(q\ r_k)\ Y_{LM}(\hat{r}_k), \text{ where } \rho^{op}(\vec{r}) = \sum_k e_k \delta(\vec{r}-\vec{r}_k), \qquad \text{(III.23)}$$

and consider the transition matrix elements $\langle J_fM_f|\ f_{LM}^{op}(q)\ |\ J_iM_i\rangle$, where $J_iM_i(J_fM_f)$ denote the initial (final) nuclear states. We then obtain the differential cross section, expression (III.17), by using the equations (III.15), (III.18), (III.22) and (III.23). Starting out with the ground state $|J_iM_i\rangle$, the operators $H_C^T(H_C)$ in $|H_C|^2$ can lead to the final states $|J_fM_f\rangle$ ( $|J_f'M_f'\rangle$). The differential cross section can, therefore, be looked upon as a "density matrix" with indices $(J_fM_f)$, $(J_f'M_f')$:

$$\left(d\sigma/d\Omega\right)^{J_i \to J_f, J_f'}_{M_i \to M_f, M_f'} = (4\pi)^2\,(2\,e^2k_2/k_1\,\Delta^4\,[J_f][J_f'])$$

$$\sum_{LM,L'M'} (J_iM_i, LM|J_fM_f)(J_iM_i, L'M'|J_fM_f)$$

$$\times\ R_{LL'}^{MM'}\ , \qquad \text{(III.24)}$$

where,

$$R_{LL'}^{MM'} = V_C(\Theta)\ Y_{L'M'}^*(\hat{q})\ Y_{LM}(\hat{q})\ (f_L^{if})^*\ f_{L'}^{if}\ , \qquad \text{(III.25)}$$

$$V_C(\theta) = (\Delta^2/q^2)^2 (E_1E_2 + \vec{k}_1.\vec{k}_2 + m_e^2) \qquad \text{(III.26)}$$

and

$$f_L^{if}(q) \equiv \langle J_f || f_L^{op}(q) || J_i \rangle = [J_f] \langle J_f M_f | f_{LM}^{op} | J_i M_i \rangle / (J_i M_i, LM | J_f M$$

(Here $[a] = (2a + 1)^{1/2}$) .

(III.27)

Finally, by setting $J_f' = J_f$, $M_f' = M_f$ and summing over final spin projections $M_f$ and averaging over the initial ones $M_i$, we obtain the differential cross section for electro-excitation ($J_i \to J_f$):

$$\left(\frac{d\sigma}{d\Omega}^{J_i \to J_f}\right)_{\text{Coulomb}} = [J_i]^{-2} \sum_{M_i, M_f} \left(\frac{d\sigma}{d\Omega}\right)^{J_i \to J_f, J_f}_{M_i \to M_f, M_f} \quad . \text{(III.28)}$$

The sums over the spin projections can be evaluated by invoking the orthogonality of the Clebsch-Gordan coefficients

$$\sum_{M_i, M_f} (J_i M_i, LM | J_f M_f)(J_i M_i, L'M' | J_f M_f) = [J_f]^2 [L]^{-1} [L']^{-1} \delta_{LL'} \delta_{MM'},$$

and the formula

$$\sum_M Y^*_{LM}(\hat{q})\, Y_{LM}(\hat{q}) = [L]^2/4\pi \quad .$$

The expression (III.24) thus yields

$$\left(\frac{d\sigma}{d\Omega}^{J_i \to J_f}\right) = (2Z^2e^2k_2/k_1\Delta^4)\, V_C(\theta)\, |F(q)|^2\, f_{\text{recoil}} \,, \text{(III.29)}$$

where

$$f_{\text{recoil}} = [1 + (2k_1/M)\, \sin^2(\theta/2)]^{-1} \quad , \qquad \text{(III.30)}$$

and the form factor $|F(q)|^2$ is defined as

$$|F(q)|^2 = (4\pi/Z^2)(2J_i+1)^{-1} \sum_L |\langle J_f || f_L^{op}(q) || J_i \rangle|^2 \quad . \tag{III.31}$$

III.2.2 Inelastic Scattering Form Factors in Terms of Projected Hartree-Fock-Bogoliubov Wavefunctions

The framework of angular momentum projection has already been given in some detail in the preceding Chapter. Here we shall just outline the method as it applies to the calculation of the C2 form factors. It may be pointed out that, although the PHFB method has earlier been successfully employed for the calculation of the level energies, static quadrupole moments and reduced transition probabilities for E2 transitions, its use in the calculation of C2 form factors has not been reported so far.

Using the projected HFB wave functions $|\Psi_K^J\rangle$ [see equation (II.57)], one obtains

$$\langle \Psi_0^{J_f} | f_{LM=0}^{op} | \Psi_0^{J_i} \rangle = [n^{J_f} n^{J_i}]^{-1/2} \int_0^{\pi/2} \sum_\mu \begin{bmatrix} J_i & L & J_f \\ -\mu & \mu & 0 \end{bmatrix} \times$$

$$\times d^{J_i}_{-\mu 0}(\theta)\ n(\theta) \{ \sum_{k\alpha\beta} e_k \langle n_\alpha l_\alpha | j_L(qr_k) | n_\beta l_\beta \rangle \times$$

$$\times \langle \alpha | Y^{(L)}_{M'} | \beta \rangle\ \rho^k_{\alpha\beta}(\theta) \} \sin\theta d\theta \quad . \tag{III.32}$$

The density matrix $\rho(\theta)$ is defined by equation (II.61).

Here the normalisations $n^J$'s are given as

$$n^J = \int_0^{\pi/2} n(\theta)\, d^J_{00}(\theta)\, \sin\theta d\theta \quad , \qquad \text{(III.33)}$$

where

$$n(\theta) = \sqrt{\det\,(1+M(\theta))} \quad . \qquad \text{(III.34)}$$

The reduced transition probability for electric quadrupole transition, $B(E2,\ 0^+ \to 2_1^+)$, and the static quadrupole moments for the first $2_1^+$ state, $Q_{2^+}$, are given by

$$B(E2,\ 0^+ \to 2_1^+) = \frac{1}{16\pi} |< \Psi_0^2 \| Q^2 \| \Psi_0^2 >|^2 \qquad \text{(III.35)}$$

and

$$Q_{2+} = < \Psi_2^2 | Q_0^2 | \Psi_2^2 > \quad , \qquad \text{(III.36)}$$

where,

$$Q^2_\mu = \sqrt{\frac{16\pi}{5}}\ (\frac{r^2}{b^2})\ Y^2_\mu(\Omega) \qquad \text{(III.37)}$$

and b is the oscillator length parameter.

The expression for the reduced matrix element appearing in eq.(III.35) can be obtained from eq.(III.32) by replacing $j_L(qr)$ by $r^L$.

The calculations were performed as follows. First, the wave functions $|\Phi_o>$ were obtained by carrying out the HFB (or the HF-BCS) calculation. The details of the intrinsic states-the amplitudes ($U_i^m$, $V_i^m$) and the expansion coefficients

$C^{m}_{ji}$ - are used to set up the f matrix (see equation (II.56)). Then F, M and 1/(1+M) appearing in equations (II.61)-(II.63), are evaluated for twenty values of the Gaussian quadrature points between the range $(0,\pi/2)$. Finally, the form factor is computed from equation (III.32).

For the evaluation of the single-particle matrix elements, we have employed the oscillator wave functions with the length parameter given by $b = 1.01 \times A^{1/6}$ fm. The center-of-mass correction[1,2] has been taken into account by multiplying a factor $\exp(b^2q^2/4A)$. The correction[2] due to the finite size of proton has been incorporated through a factor $\exp(-a_p^2q^2/4A)$ where $a_p = 0.59$ fm.

Further, in order to compare the form factor calculated by PWBA with the experiment, the experimental data have been plotted at the effective momentum transfer[7] $q_{eff}$ instead of the kinematic q:

$$q_{eff} = q\left[1 + \frac{3\sqrt{3}}{2\sqrt{5}}\frac{Ze^2}{ER}\right] , \qquad \text{(III.38)}$$

where R is the rms radius and E is the energy of the incident electrons.

### III.2.3 The Input Parameters of the Calculation

In our calculations we have employed the MWH effective interaction[9,10] described in the preceding Chapter. As

demonstrated earlier, this effective interaction is quite appropriate from the point of view of the subshell occupation numbers as well as the deformation trends[11] in the 2p-1f shell. The single-particle energies for the 2p-1f shell orbits are taken from the $^{41}$Ca spectrum:

$\varepsilon(1f_{7/2}) = 0.0$, $\varepsilon(2p_{3/2}) = 2.1$ MeV, $\varepsilon(2p_{1/2}) = 3.9$ MeV, and $\varepsilon(1f_{5/2}) = 6.5$ MeV.

III.2.4 The Intrinsic States for N=28 and N≠28 Isotopes

We have obtained the axially symmetric intrinsic states for the N≠28 nuclei $^{46,48}$Ti, $^{50}$Cr and $^{56}$Fe by following the HFB procedure discussed in Refs.12-14. Pairing correlations between only the like particles are allowed in our calculations. For the N=28 nuclei $^{50}$Ti, $^{52}$Cr and $^{54}$Fe, however, we have employed the deformed HF-BCS procedure discussed by Goodman[15]. It turns out that, whereas the HFB prescription leads to intrinsic states possessing sizable quadrupole deformations in the case of the N≠28 nuclei, it yields nearly spherical intrinsic states in the nuclei with N=28 closed shell. This is because the HFB framework, which is expected to treat the deformation and the pairing effects on the same footing, overemphasizes the latter whenever a subshell closure is possible. The near-sphericity of the N=28 HFB states implies vanishingly small (<10%) amplitudes for angular momentum states with J≠0, a feature which renders them unsuitable in the

context of the present calculation which requires a satisfactory description of both the J=0 as well as J=2 states. The HF-BCS intrinsic states for the N=28 nuclei, on the other hand, are quite deformed.

III.3 Results and Discussion

Since the $J^{\pi} = 0^+, 2^+$ states projected from the HFB intrinsic wave function consist dominantly of $(1f_{7/2}, 2p_{3/2})^n$ configurations, the matrix elements $\langle f|j_2(qr)|f\rangle$ and $\langle f|j_2(qr)|p\rangle$ are expected to play important roles vis-à-vis the observed squared form factors; in fact the gross qualitative features, viz. the appearance of two maxima at $q \sim 0.7$ $fm^{-1}$ and $q \sim 1.7$ $fm^{-1}$, can be understood in terms of the q-dependence of these matrix elements. With the assumption that the q-dependence of these matrix elements is not altered significantly by the effective charge, it turns out that (see Fig.III.1), whereas the matrix element $|\langle f|j_2(qr)|f\rangle|$ possesses maxima at $q \sim 0.8$ $fm^{-1}$ and $q \sim 1.9$ $fm^{-1}$, the maxima of the matrix element $|\langle f|j_2(qr)|p\rangle|$ occur at $q \sim 0.7$ $fm^{-1}$ and $q \sim 1.6$ $fm^{-1}$. The zeros of the matrix elements $\langle f|j_2(qr)|f\rangle$ and $\langle f|j_2(qr)|p\rangle$ occur at $q \sim 1.6$ $fm^{-1}$ and $q \sim 1.2$ $fm^{-1}$, respectively. Since F(q) involves (see Eq.(III.32)) a linear combination of the matrix elements $\langle f|j_2(qr)|f\rangle$ and $\langle f|j_2(qr)|p\rangle$, it is expected to exhibit two maxima in the ranges $q = (0.7, 0.8)$ $fm^{-1}$ and $q = (1.6, 1.9)$ $fm^{-1}$, as well as a zero in the range $q = (1.2, 1.6)$ $fm^{-1}$. This is consistent

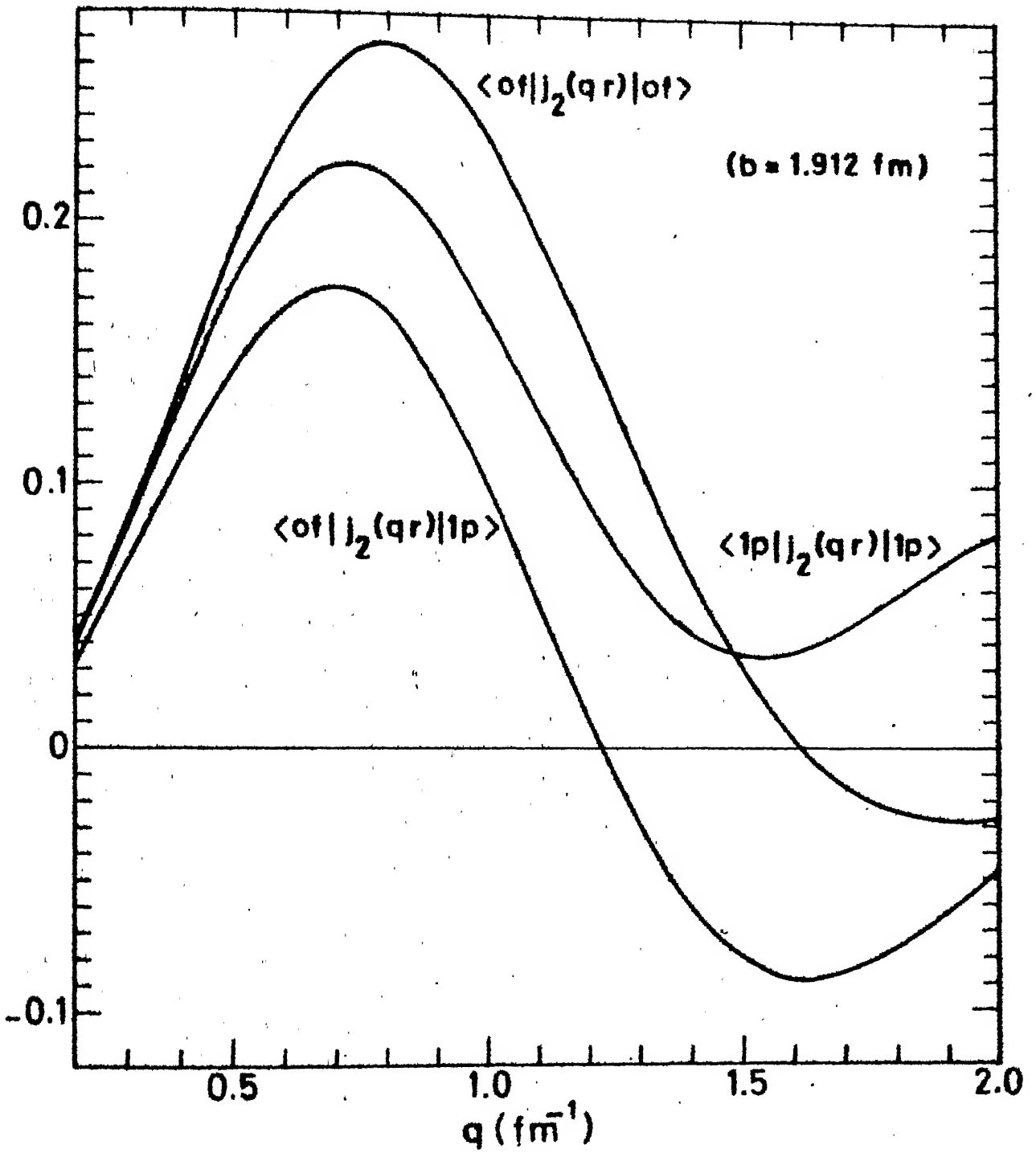


FIG. III.1 THE MOMENTUM-TRANSFER DEPENDENCE OF THE MATRIX ELEMENTS OF $j_2(qr)$ IN THE OSCILLATOR BASIS.

with the observed features of $|F(q)|^2$ in various 2p-1f shell nuclei.

III.3.1 N=28 Isotones

The squared form factors $|F(q)|^2$ for the $0^+ \rightarrow 2_1^+$ transitions in the N=28 isotones are calculated and compared with the experiments in Fig.III.2.

In our calculations we employed the effective charges $e_p = 1.7e$ for protons and $e_n = 0.7e$ for neutrons for the three nuclei $^{50}Ti$, $^{52}Cr$ and $^{54}Fe$. As we shall see later, this set of effective charges is consistent with the available electromagnetic properties involving the $0^+$ and $2_1^+$ states of these nuclei. From the results presented in Fig. III.2, one finds that the overall quantitative agreement of the calculated form factors with the experiments is reasonably good, particularly in view of the fact that the effective charges were not fine-tuned for each isotone.

A noticeable discrepancy, however, occurs in the case of the nucleus $^{54}Fe$ for $q_{eff} > 1.4$ fm$^{-1}$; the present calculation underestimates the magnitude of the form factor at the second peak around $q_{eff} \sim 1.7$ fm$^{-1}$ by about 34 percent. This may be due to the inadequacy of PWBA for large $q_{eff}$ and/or, insufficient configurational admixtures in the HF-BCS wave functions in $^{54}Fe$; the latter feature is also reflected in the low value of the contribution of neutrons towards the total

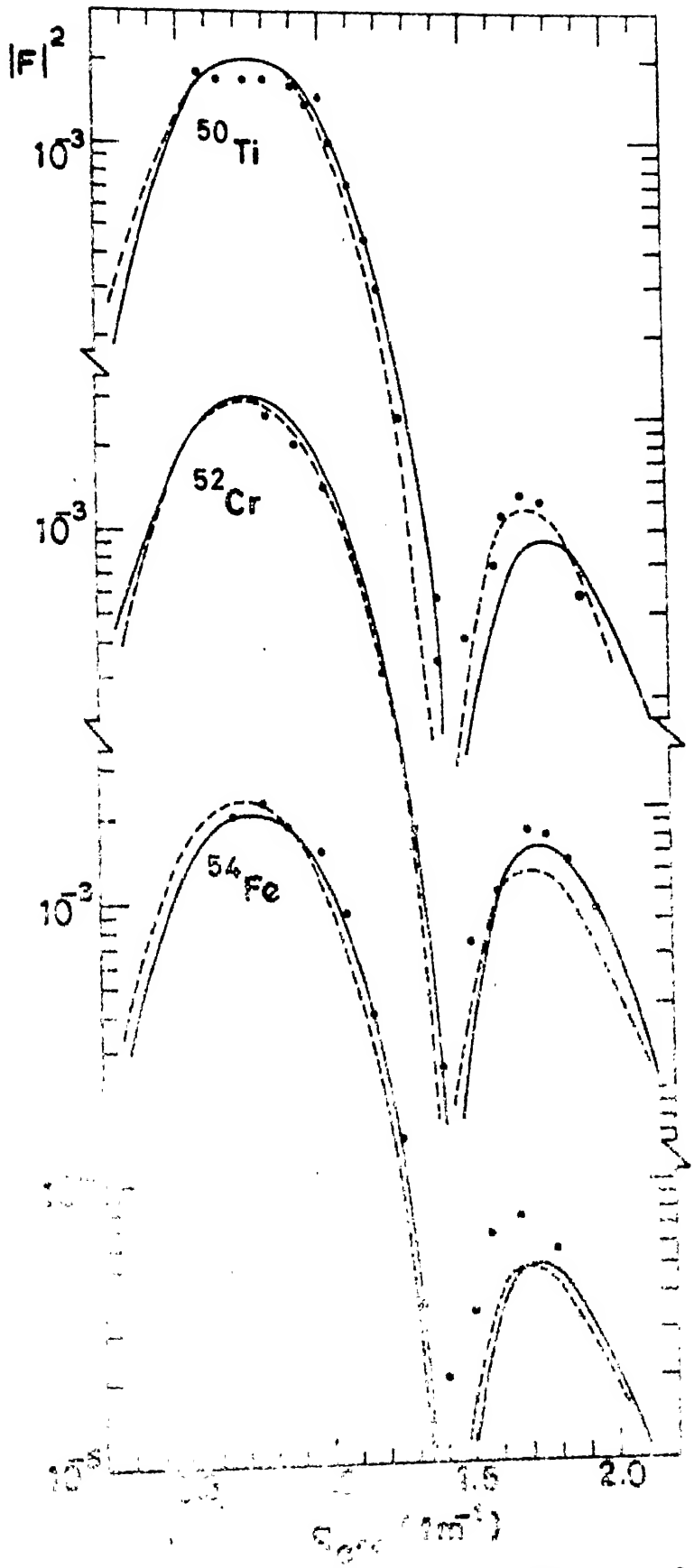


FIG. III.2 THE EXPERIMENTAL AND CALCULATED SQUARED FORM FACTORS FOR THE $0^+ \rightarrow 2_1^+$ TRANSITIONS IN THE N = 28 ISOTONES

intrinsic quadrupole moment for $^{54}$Fe (see column 2, Table III.1).

We have also given in Fig. III.2 the results obtained by Iwamoto et al.[7] in the framework of shell model involving the $f_{7/2}^{n} + f_{7/2}^{n-1} p_{3/2}$ configurations. The effective charges $(e_p, e_n) = (1.4e, 1.0e)$, $(1.6e, 1.2e)$ and $(1.8e, 1.4e)$ were employed for the nuclei $^{50}$Ti, $^{52}$Cr and $^{54}$Fe, respectively, in these calculations.

It is seen that whereas the PHFB results are quite close to the shell model ones in the nucleus $^{54}$Fe, they show distinct improvement over the latter in case of the nucleus $^{52}$Cr. The shell model calculations, however, yield better agreement with the experiments than the PHFB ones in case of the nucleus $^{50}$Ti. It may be pointed out that the shell model calculation involved an independent variation of both the effective charges $(e_p, e_n)$ to fit the two maxima of $|F|^2$ for the nucleus $^{50}$Ti. The effective charges for $^{52}$Cr and $^{54}$Fe were, however, determined by varying only the isoscalar charge, $\frac{1}{2}(e_p + e_n)$, so as to fit the lower-momentum transfer region of $|F|^2$ while the isovector charge, $\frac{1}{2}(e_p - e_n)$, was kept fixed to that used in $^{50}$Ti.

### III.3.2 The Nuclei $^{46,48}Ti$, $^{50}Cr$ and $^{56}Fe$

Fig. III.3 compares the calculated and the experimental $|F|^2$ for the $0^+ \rightarrow 2_1^+$ transitions in the nuclei $^{46,48}Ti$, $^{50}Cr$ and $^{56}Fe$. Iwamoto et al.[7] had carried out shell-model calculations for the nuclei $^{46,48}Ti$ and $^{52}Cr$; we have also shown their results here for the sake of comparison. However, no calculations on form factors has so far been reported for the nucleus $^{56}Fe$.

As in the calculations reported in the previous section, the effective charges have been used such that the proton effective charge is always greater than the neutron effective charge by an amount e. Here we find that the form factors resulting from the PHFB wave functions are in strikingly good overall agreement with the experiments provided a reasonable variation of the effective charges - with $e_n$ ranging between 0.5 and 0.7 — is allowed. Thus, the values for proton and neutron effective charges that we have employed are $(e_p, e_n) = (1.7e, 0.7e)$ for $^{48}Ti$, $(1.6e, 0.6e)$ for $^{46}Ti$ and $^{50}Cr$, and $(1.5e, 0.5e)$ for the nucleus $^{56}Fe$. With these effective charges, the maximum discrepancy is seen to occur in the case of the nucleus $^{56}Fe$ for $q_{eff} > 1.4$ fm$^{-1}$ where the present calculation underestimates the magnitude of the second peak by about 18 percent.

In the nuclei $^{46,48}Ti$ and $^{50}Cr$, the form factors resulting from the PHFB wave functions show significant improvement over

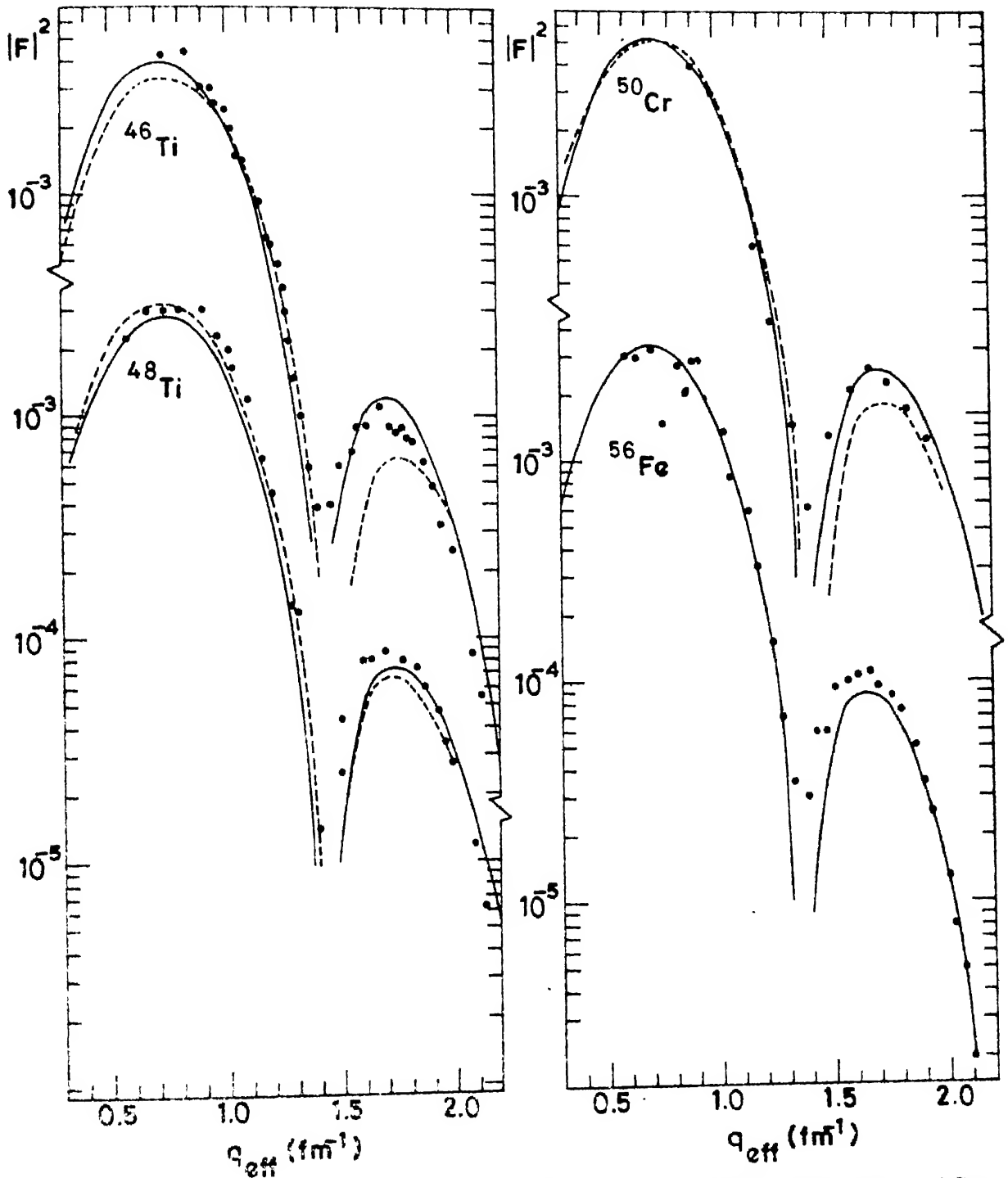


FIG. III . 3 THE EXPERIMENTAL AND CALCULATED SQUARED FORM FACTORS FOR THE $0^+ \longrightarrow 2_1^+$ TRANSITIONS IN $^{46,48}Ti$, $^{50}Cr$ AND $^{56}Fe$

TABLE III.1

The $Q_{2^+}$ and $B(E2; 0^+ \rightarrow 2_1^+)$ values for some Ti, Cr and Fe isotopes calculated with $e_n = 0.5e$, $e_n = 0.6e$, as well as $e_n = 0.7e$ (with $e_p = e_n + e$) are tabulated. The $B(E2; 0^+ \rightarrow 2_1^+)$ values are in units of $e^2.fm^4$ and the $Q_{2^+}$ values have been given in units of $e.fm^2$. Here $\langle Q_o^2 \rangle_\pi$ ($\langle Q_o^2 \rangle_\nu$) gives the contribution of the valence protons (neutrons) to the intrinsic state.

| Nucleus | $Q_o^2$ $[\langle Q_o^2\rangle_\pi, \langle Q_o^2\rangle_\nu]$ | B (E2) (Calc.) $e_n=0.5$ | $e_n=0.6$ | $e_n=0.7$ | B(E2) (Expt.)[a] | $Q_{2^+}$ (Calc.) $e_n=0.5$ | $e_n=0.6$ | $e_n=0.7$ | $Q_{2^+}$ (expt.)[a] |
|---|---|---|---|---|---|---|---|---|---|
| $^{46}$Ti | 22.6 [9.2,13.3] | 662 | 815 | 983 | 855±40<br>1070±100 | -23.1 | -25.6 | -23.2 | -21±6<br>-19±10 |
| $^{48}$Ti | 16.7 [6.8,9.9] | 364 | 451 | 547 | 690±60<br>750±50 | -16.1 | -13.0 | -19.8 | -13±6<br>-13.5±8.8 |
| $^{50}$Ti | -8.4 [-4.4,-4.0] | 265 | 320 | 378 | 330±40<br>315±30 | 10.5 | 11.5 | 12.5 | 8±16<br>-2±9 |
| $^{50}$Cr | 25.5 [12.7,12.8] | 1077 | 1302 | 1547 | 1040±115<br>1135±100 | -29.5 | -32.4 | -35.3 | -36±7 |
| $^{52}$Cr | 11.6 [8.0,3.6] | 534 | 627 | 727 | 565±50<br>660±30 | -15.0 | -16.2 | -17.5 | -14±8 |
| $^{54}$Fe | 9.1 [6.5,2.6] | 442 | 518 | 600 | 535±40<br>675±40[b] | -15.7 | -16.9 | -18.1 | -5±14[b] |
| $^{56}$Fe | 25.5 [11.9,13.6] | 1100 | 1341 | 1606 | 970±20[c] | -29.8 | -32.9 | -36.0 | -24±3[c] |

[a] Experimental data are taken from Ref.16

[b] Ref. 17

[c] Ref. 18.

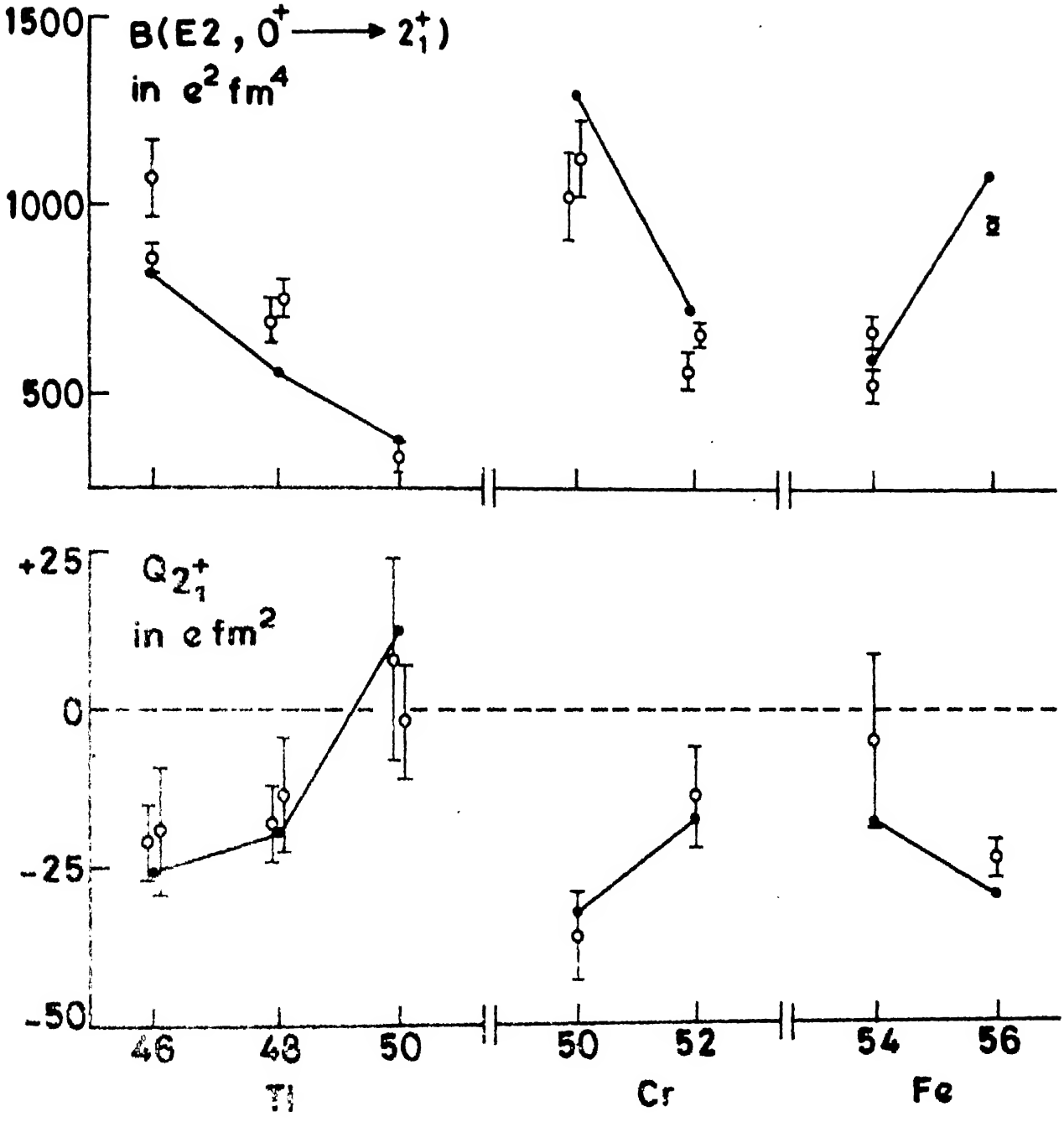


FIG. III.4 THE E2 TRANSITION STRENGTHS AND STATIC QUADRUPOLE MOMENTS IN SOME Ti, Cr AND Fe ISOTOPES.

form factors, yield B(E2) and $Q_{2^+}$ values which are consistent with the currently available experimental information for all the nuclei considered here.

## III.4 Conclusions

We have presented here the calculation of Coulomb form factors for the $0^+ \rightarrow 2_1^+$ transition in some doubly even Ti, Cr and Fe isotopes in terms of the projected HFB wavefunctions. In keen contrast with the results obtained in some recent shell model calculations involving $f_{7/2}^n + f_{7/2}^{n-1} p_{3/2}$ configurations, it is seen that the use of the self-consistent projected HFB wave functions resulting from a slightly modified version of the Kuo-Brown interaction for the 2p-1f shell leads not only to a significant overall improvement in the calculated form factors, it also obviates the necessity of using widely different effective charges for various nuclei. However, the application of Distorted Wave Born Approximation (DWBA) instead of PWBA employed in the present work, is likely to result in further improvements in the magnitudes of the calculated form factors around the second maxima.

In view of the intractability of large-scale shell model calculations in the 2p-1f shell nuclei, the method employed in the present work is expected to provide a reliable alternative for obtaining a reasonably accurate microscopic description of the observed data on C2 form factors.

## REFERENCES


1. T. de Forest and J. Walecka, Adv. Phys. 15, 1 (1966).

2. H. Überall, Electron Scattering From Complex Nuclei, (Academic, New York 1971).

3. J. Heisenberg, J.S. McCarthy and I. Sick, Nucl. Phys. A164, 353 (1971).

4. K. Hosoyama et al., Res. Rep. Nucl. Sci. (Tohoku University) 7, 279 (1974); 8, 55 (1975).

5. K. Hosoyama et al., Res. Rep. Nucl. Sci. (Tohoku University) 11, 1 (1978).

6. J.W. Lightbody, Jr. et al., Bull. Am. Phys. Soc. 20, 568 (1975).

7. T. Iwamoto, H. Horie and A. Yokoyama, Phys. Rev. C25, 658 (1982).

8. J.D. Bjorken and S.D. Drell, Relativistic Quantum Mechanics (McGraw Hill, New York, 1964), p. 33.

9. T.T.S. Kuo and G.E. Brown, Nucl. Phys. A114, 241 (1968).

10. J.B. McGrory, B.H. Wildenthal and E.C. Halbert, Phys. Rev. C2, 186 (1970).

11. S.K. Sharma and K.H. Bhatt, Phys. Rev. Lett. 30,620 (1973).

12. C. Bloch and A. Messiah, Nucl. Phys. 39, 95 (1962); S.B. Khadikikar and M.R. Gunye, ibid A144, 289 (1970).

13. N. Onishi and S. Yoshida, Nucl. Phys. 80, 376 (1966).

14. S.K. Sharma, Nucl. Phys. A260, 226 (1976).

15. A.L. Goodman in Advances in Nuclear Physics, edited by J.W. Negele and E. Vogt (Plenum Press, New York - London 1979), Vol. 11, p. 263.

16. W. Kutschera, in Proceedings of the Topical Conference on Physics of Medium - Light Nuclei, Florence, 1977, edited by P. Blasi and R.A. Ricci (Editrice Compositori, Bologna, 1978), p. 120.

17. M.J. Levine, E.K. Warburton, and D. Schwalm, Phys. Rev. C23, 244 (1981).

18. A. Christy and O. Häusser, Nucl. Data Tables 11, 281 (1972).

# CHAPTER IV

## INELASTIC ELECTRON SCATTERING FORM FACTORS INVOLVING THE NON-YRAST $2^+$ LEVELS IN THE NUCLEI $^{48}Ti$, $^{50}Cr$ AND $^{54,56}Fe$

### IV.1 Introduction

Some recent inelastic electron scattering experiments[1-4] have provided valuable data on the $0^+ \rightarrow 2_2^+$ transitions in the nuclei ($^{48}Ti$, $^{50}Cr$, $^{54}Fe$) and the $0^+ \rightarrow 2_3^+$ transition in the nucleus $^{56}Fe$. Although the qualitative features of the observed form factors associated with the $0^+ \rightarrow 2_{2,3}^+$ transitions are quite similar to those of the observed form factors for the $0^+ \rightarrow 2_1^+$ transitions discussed in the preceding Chapter, the magnitudes of $|F|^2$ for the former transitions are smaller by an order of magnitude than those for the latter.

In this Chapter we discuss an extension of the formalism presented earlier with a view to provide an interpretation of the available form factors involving the non-yrast $2^+$ levels in the nuclei $^{48}Ti$, $^{50}Cr$ and $^{54,56}Fe$.

Recently Iwamoto *et al.*[5] have also studied the C2 form factors involving the second excited $2^+$ states in some Ti and Cr isotopes in terms of the wave functions resulting from empirical effective interactions operating in the restricted valence space consisting of the $f_{7/2}^n + f_{7/2}^{n-1} p_{3/2}$ configurations. In their work Iwamoto *et al.*[5] employed the empirical

effective interactions given by Oda et al.[6] as well as by Yokoyama et al.[7]. As discussed in the preceding chapter, the results for the low momentum-transfer ($q_{eff} < 1.5$ fm$^{-1}$) region of $|F|^2$ ($0^+ \rightarrow 2_1^+$) were consistent with experiments; the results were also quite stable towards the choice of different effective interactions. However, the choice of the $f_{7/2}^n + f_{7/2}^{n-1} p_{3/2}$ space proved too restrictive to permit an unambiguous interpretation of the available data for the high momentum-transfer part of the $0^+ \rightarrow 2_1^+$ transition, as well as the $0^+ \rightarrow 2_2^+$ transition involving $0.5$ fm$^{-1} < q_{eff} < 2.0$ fm$^{-1}$; the calculated results displayed large variation with respect to the choice of the effective interactions. Furthermore, none of the two effective interactions yielded acceptable simultaneous agreement for the $0^+ \rightarrow 2_1^+$ as well as the $0^+ \rightarrow 2_2^+$ transitions, although relatively large values of the neutron effective charges — $e_n = 1.0e$ and $e_n = 1.2e$ for the nuclei $^{48}$Ti and $^{50}$Cr, respectively — were employed.

As we have already seen, the yrast wave functions projected from the HFB intrinsic states of prolate snapes resulting from the modified version of the KB effective interaction[8,9] for the full 2p-1f space provide a good description of the observed form factors for the $0^+ \rightarrow 2_1^+$ transitions in several 2p-1f shell nuclei[10]. Here we show that a fairly satisfactory interpretation of the available $|F|^2$ data for the $0^+ \rightarrow 2_2^+$ transitions in the nuclei ($^{48}$Ti, $^{50}$Cr, $^{54}$Fe) and the $0^+ \rightarrow 2_3^+$ transition in the nucleus $^{56}$Fe can also be

attempted in terms of reasonable values of the proton and neutron effective charges by describing the yrare and yr states in terms of the oblate variational solutions resulting from the modified KB interaction[11].

In section IV.2 we discuss the details of the calculational framework. In section IV.3 we present the comparison of the calculated $0^+ \rightarrow 2^+_{2,3}$ form factors with the experiments. Finally section IV.4 contains some concluding remarks.

## IV.2 Calculational Framework

The details concerning the calculation of the inelastic scattering form factors for the $0^+ \rightarrow 2^+_1$ transition in terms of the states with $J = 0,2$ projected from the same intrinsic HFB state (with K=0) have already been discussed in section III.2.2. However the states with J=0,2 involved in the calculation of the $0^+ \rightarrow 2^+_{2,3}$ form factors necessarily belong to two different intrinsic states; whereas the J=0 belongs to the yrast band, the states $J = 2_2$ ($2_3$) belong to the yrare (yr ) band. Further, as discussed later, the yrast and the non-yrast bands belong to the prolate and oblate intrinsic states, respectively, in the nuclei considered in this Chapter.

The eigenstates of $\hat{J}^2$ projected from the HFB state $|\Phi_K(\delta)>$ can be written as

$$|JK(\delta)> = P^J_{KK} |\Phi_K(\delta)> = \frac{2J+1}{8\pi^2} \int D^J_{KK}(\Omega)\ R(\Omega) |\Phi_K(\delta)> d\Omega \ , \qquad (IV.1)$$

where $R(\Omega)$ and $D^{J}_{KK}(\Omega)$ are the rotation operator and the rotation matrix, respectively. Here $\delta$ denotes the type (prolate or oblate) of quadrupole deformation of the intrinsic state.

The intrinsic state $|\Phi_K(\delta)>$ can be written as (Eq. II.44)

$$|\Phi_K(\delta)> = \prod_{im} (U^m_i(\delta) + V^m_i(\delta)\ b^\dagger_{im}\ b^\dagger_{\bar{i}m})|o> \quad , \qquad (IV.2)$$

where the creation operator $b^\dagger_{im}$ can be expressed as

$$b^\dagger_{im} = \sum_j C^m_{ji}(\delta)\ a^\dagger_{jm}; \quad b^\dagger_{\bar{i}m} = \sum_j C^m_{ji}(\delta)\ (-1)^{j-m}\ a^\dagger_{j-m} \ . \qquad (IV.3)$$

As before, here j labels the spherical single-particle orbits $(1f_{7/2},\ 2p_{3/2},\ 2p_{1/2},\ 1f_{5/2})$.

The PWBA expression for the squared form factor $|F|^2$ involved in the Coulomb scattering is in this case given by[12]

$$|F(q)|^2 = \frac{4\pi}{Z^2}\ \frac{1}{(2J_i+1)}\ |<J_f(\delta_2)||\hat{f}_L||J_i(\delta_1)>|^2 \quad , (IV.4)$$

where Z is the atomic number of the target nucleus. Here $J_i(\delta_1)$ and $J_f(\delta_2)$ denote the initial and the final scattering states resulting from angular momentum projection on the intrinsic states $|\Phi_K(\delta_1)>$ and $|\Phi_K(\delta_2)>$, respectively. The one-body operator $\hat{f}_{LM}$ is given by the eqn.(III.23).

The expression for the matrix element $\langle J_f(\delta_2) | \hat{f}_{LM} | J_i(\delta_1) \rangle$ is as follows:

$$\langle J_f(\delta_2) | \hat{f}_{L\mu} | J_i(\delta_1) \rangle = [n^J(\delta_1) n^{J'}(\delta_2)]^{-1/2} \int_0^{\pi/2} \sum_{\mu} \begin{bmatrix} J & 2 & J' \\ -\mu & \mu & 0 \end{bmatrix} d^J_{\mu 0}(\Theta)$$

$$\times\, n(\delta_1, \delta_2, \Theta) b^2 [\sum_{\tau_3 \alpha\beta} e_{\tau_3} \langle \alpha | \hat{f}_{L\mu} | \beta \rangle \rho^{\tau_3}_{\alpha\beta}(\delta_1, \delta_2, \Theta)] \sin\Theta d\Theta \,, \tag{IV.5}$$

where

$$n^J(\delta) = \int_{\delta}^{\pi} [\det(1+F(\delta,\Theta)\, f^{\dagger}(\delta))]^{1/2} d^J_{00}(\Theta) \sin\Theta d\Theta \,, \tag{IV.6}$$

$$n(\delta_1, \delta_2, \Theta) = [\det(1+F(\delta_1,\Theta) f^{\dagger}(\delta_2))]^{1/2} \tag{IV.7}$$

and

$$\rho^{\tau_3}_{\alpha\beta}(\delta_1, \delta_2, \Theta) = [M(\delta_1,\delta_2,\Theta)/(1+M(\delta_1,\delta_2,\Theta))]^{\tau_3}_{\alpha\beta} \,, \tag{IV.8}$$

with $$M(\delta_1,\delta_2,\Theta) = F(\delta_1,\Theta) f^{\dagger}(\delta_2) \,. \tag{IV.9}$$

The matrices $f^{\dagger}$ and F are defined by equations analogous to the ones given earlier (see Eqs.II.56 and II.63):

$$f_{\alpha\beta}(\delta) = \sum_i C^{m_\alpha}_{j_\alpha i}(\delta)\, C^{m_\beta}_{j_\beta i}(\delta)\, \frac{v^{m_\alpha}_i}{v^{m_\alpha}_i}\, \delta_{m_\alpha, -m_\beta} \tag{IV.10}$$

and

$$F_{\alpha\beta}(\delta,\Theta) = \sum_{m'_\alpha m'_\beta} d^{j_\alpha}_{m_\alpha m'_\alpha}(\Theta)\, d^{j_\beta}_{m_\beta m'_\beta}(\Theta)\, f_{\alpha\beta}(\delta) \,. \tag{IV.11}$$

The calculations were performed as follows. First the wavefunctions $\Phi_o(\delta_1)$ and $\Phi_o(\delta_2)$ were obtained, for the yrast and

the yrare (or yr ) bands respectively, by carrying out the HFB (or the HF) calculations. The amplitudes ($U_i^m(\delta)$, $V_i^m(\delta)$) and the expansion coefficients $C_{ji}^m(\delta)$ were used to set up the $f(\delta)$ matrices. Then $F(\delta,\theta)$, $M(\delta_1,\delta_2,\theta)$ and $1/[1+M(\delta_1,\delta_2,\theta)]$ matrices were evaluated for twenty values of the Gaussian quadrature points between the range $(0,\pi/2)$. The form factor was then computed from equation (IV.5).

The centre-of-mass correction and the proton-finite-size effect have been taken into account by multiplying factors identical to the ones employed in the preceding Chapter.

## IV.3 Results and Discussion

Table IV.1 summarizes our results concerning the variational solutions associated with the (yrast, yrare) levels in the nuclei ($^{48}$Ti, $^{50}$Cr, $^{54}$Fe) and the (yrast, yr ) levels in the nucleus $^{56}$Fe.

In the case of the nuclei $^{48}$Ti and $^{54}$Fe, the excited, self-consistent solutions of either the HFB or the HF-BCS type do not exist; the inclusion of pairing correlations always leads one to the variational solution belonging to the yrast band, irrespective of the choice of the starting guess for the wavefunctions. The non-yrast states have, therefore, been projected from the (excited) HF solutions in these nuclei.

TABLE IV.1

Details of the variational intrinsic states associated with the low-lying levels in the nuclei $^{48}Ti$, $^{50}Cr$ and $^{54,56}Fe$. Here $\langle Q_o^2\rangle_\pi$ ($\langle Q_o^2\rangle_\nu$) gives the contribution (in units of $b^2$) of protons (neutrons) towards the total quadrupole moment. The entries presented in the last column represent the energy difference $[E(2_2^+)-E(2_1^+)]$ in the case of the nuclei ($^{48}Ti$, $^{50}Cr$, $^{54}Fe$), and the energy difference $[E(2_3^+)-E(2_1^+)]$ in the case of the nucleus $^{56}Fe$

| Nucleus | Type of variational solution | | $\langle Q_o^2\rangle$ ($\langle Q_o^2\rangle_\pi$, $\langle Q_o^2\rangle_\nu$) | E(MeV) | [E(I)-E(II)] | $[E(2^+_{ex})-E(2^+_1)]$ Expt. |
|---|---|---|---|---|---|---|
| | deformation | method | | | | |
| $^{48}Ti$ | I.Prolate | HFB | 16.7(6,8,9.9) | -17.53 | 1.36 | 1.44 |
| | II.Oblate | HF | -13.7(-6.0,-7.7) | -16.17 | | |
| $^{50}Cr$ | I.Prolate | HFB | 25.5(12.7,12.8) | -29.94 | 1.84 | 2.14 |
| | II.Oblate | HFB | -12.7(-6.5,-6.2) | -28.10 | | |
| $^{54}Fe$ | I.Prolate | HF-BCS | 9.0(6.4,2.6) | -46.35 | 1.32 | 1.55 |
| | II.Oblate | HF | -7.2(-5.1,-2.1) | -45.03 | | |
| $^{56}Fe$ | I.Prolate | HFB | 25.5(11.9,13.6) | -47.73 | 1.65 | 2.11 |
| | II.Oblate | HFB | -13.1(-5.7,-7.4) | -46.08 | | |

Further, as mentioned in the preceding Chapter, a description of the yrast states in $^{54}$Fe in terms of the HF-BCS (rather than HFB) solution is necessitated because of the shell closure at N=28.

The suitability of the variational solutions considered here vis-à-vis the description of various yrast as well as non-yrast $2^+$ levels can be judged from the following considerations. It is reasonable to assume that the difference in the variational energies of two solutions represents roughly the difference in the energies of the $2^+$ states projected from these solutions, provided the two solutions have nearly the same absolute value of the quadrupole moment. From the results presented in column 6 and 7, Table IV.1, we note that the variational solutions obtained in the nuclei $^{48}$Ti and $^{54}$Fe satisfy this requirement - the $|\langle Q_o^2 \rangle|$ values for the prolate and oblate solutions do not differ much. Thus the relative separations of the non-yrast and yrast $2^+$ states suggested by the intrinsic energies are about 1.4 MeV and 1.3 MeV, respectively, for the nuclei $^{48}$Ti and $^{54}$Fe. It is satisfying to observe that these estimates are quite close to the observed separations between the various $2^+$ states in these nuclei.

The difference in the energy of an intrinsic state and that of the $2^+$ state projected from it depends on the magnitude of deformation of the intrinsic state. In the case of the nuclei $^{50}$Cr and $^{56}$Fe the intrinsic deformation of

the minimum-energy solutions are significantly larger than those of the excited variational solutions. This suggests a larger value of the difference $[E_{HFB}(\text{Prolate})-E(J=2_1)]$ compared to the difference $[E_{HFB}(\text{Oblate})-E(J=2_2)]$. Consequently, the separation between the yrare/yr $2^+$ state and the yrast $2^+$ state is expected to be somewhat larger than the difference in the corresponding intrinsic energies. Keeping this in mind, it is seen that the differences in the calculated variational energies for the nuclei $^{50}Cr$ and $^{54}Fe$ are remarkably consistent with the observed relative energies of the $2^+$ states.

In the form factor calculations presented here we have employed the A-independent effective charges $(e_p, e_n) = (1.4e, 0.4e)$ for the transitions $0^+ \rightarrow 2^+_{2,3}$. These values of effective charges are somewhat smaller than the ones employed in our calculations of the $0^+ \rightarrow 2^+_1$ form factors presented in Chapter III. The reduction in the values of the effective charges in going from the yrast $2^+$ states to non-yrast $2^+$ states is not entirely unexpected since the states $2^+_1$ are usually more susceptible to core-polarization effects compared to the states $2^+_{2,3}$.

Figure IV.1 compares the calculated and experimental[2,4] $|F|^2$ for the $0^+ \rightarrow 2^+_1$ as well as $0^+ \rightarrow 2^+_2$ transitions in the nucleus $^{48}Ti$. We have also given here the results obtained by Iwamoto et al.[5] in the framework of the shell model involving

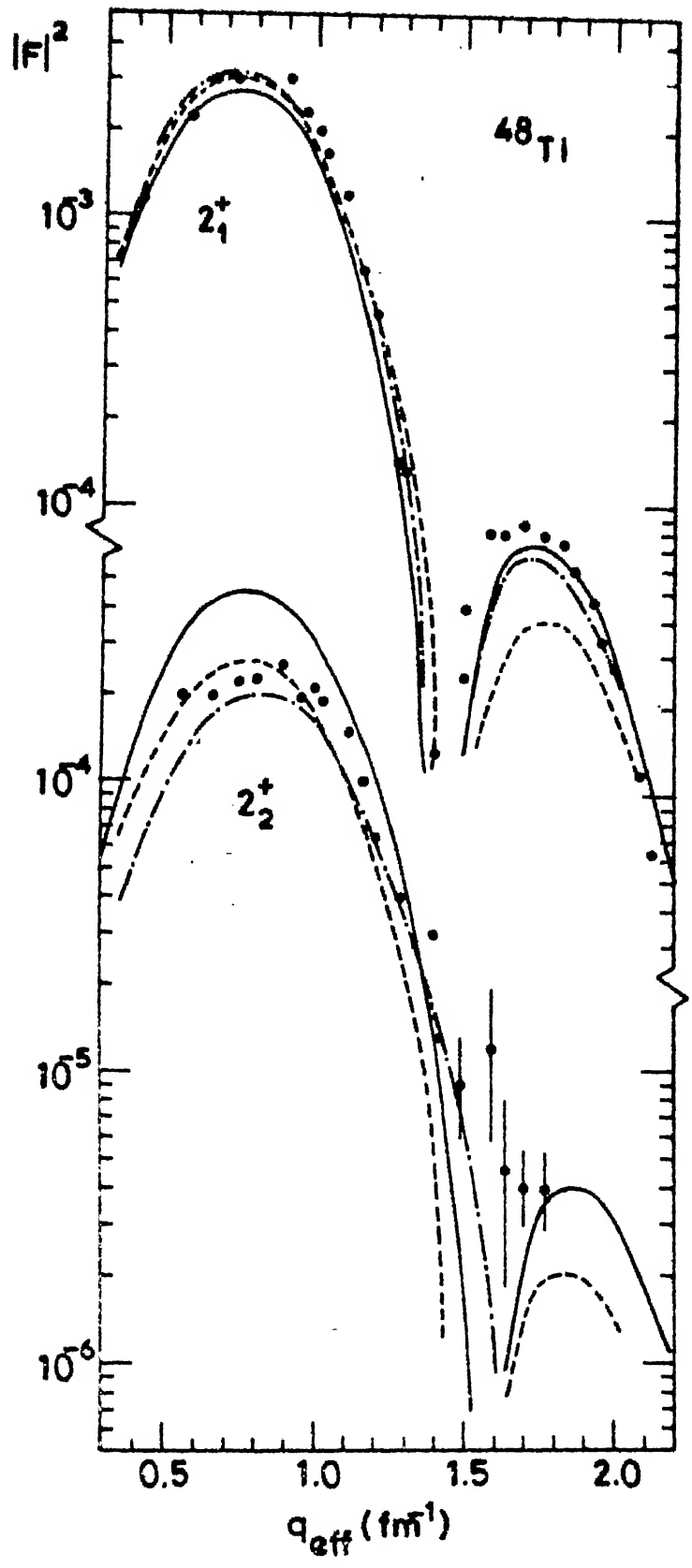


FIG.IV.1 THE EXPERIMENTAL AND CALCULATED SQUARED FORM FACTORS FOR THE $0^+ \longrightarrow 2^+_{1,2}$ TRANSITION IN $^{48}Ti$.

the $f_{7/2}^{n} + f_{7/2}^{n-1} p_{3/2}$ configurations. In the earlier work two sets of empirical effective interactions were employed. One was the set of matrix element obtained by Oda et al.[6] through a chi-square fit to the 38 levels chosen from Ca and Sc isotopes, and the other was the set obtained by Yokoyama et al.[7] through a fit to the 63 data selected from the N=27 and 28 isotones (A = 47-55). Hereafter we shall refer to these sets of matrix elements as the V(Ca-Sc) and the V(27-28) interactions, respectively. The broken and the dotted-dashed curves represent the results obtained by Iwamoto et al.[5] with the empirical effective interactions V(27-28) and V(Ca-Sc), respectively, in conjunction with the $f_{7/2}^{n} + f_{7/2}^{n-1} p_{3/2}$ configurations. The solid curves give the results obtained in the present calculation.

The results presented in Fig.IV.1 bring out the sensitivity of the restricted shell model calculations for the nigh momentum-transfer part of the form factors associated with the $0^+ \rightarrow 2^+_{1,2}$ transitions towards the choice of the effective interactions. Further, none of the effective interactions employed earlier in conjunction with the $f_{7/2}^{n} + f_{7/2}^{n-1} p_{3/2}$ space provides an adequate simultaneous interpretation of the available data involving both the $0^+ \rightarrow 2^+_1$ as well as the $0^+ \rightarrow 2^+_2$ transitions. Whereas the interaction V(Ca-Sc) leads to reasonable agreement with the experiments for $q_{eff} > 1.5$ fm$^{-1}$ in the case of the $0^+ \rightarrow 2^+_1$ transition, the calculated values (not shown in the figure) for high momentum-transfer involving the

$0^+ \rightarrow 2_2^+$ transition are smaller by more than an order of magnitude. The shell model estimates for $|F|^2$ around its second maximum obtained with the interaction V(27-28), on the other hand, are smaller than the observed ones by roughly a factor of two for the $0^+ \rightarrow 2_1^+$ as well as the $0^+ \rightarrow 2_2^+$ transitions.

It is seen that the present calculation yields an adequate overall quantitative description of the available data for both the $0^+ \rightarrow 2_1^+$ as well as the $0^+ \rightarrow 2_2^+$ transitions. In particular, the PHFB values for the squared form factor around $q_{eff} = 1.7$ fm$^{-1}$ show substantial improvements over the earlier results. Our choice of the neutron effective charge also contrasts keenly with the values employed in the earlier work; the present calculation involves the effective charge $e_n = 0.4e$ whereas the restricted shell model calculation employed $e_n = 1.0e$. The proton effective charge employed in the earlier calculation is, however, the same as the one used in the present one.

A significant discrepancy between the calculated and the observed results occurs around the first maximum associated with the $0^+ \rightarrow 2_2^+$ transition where the PHFB results overestimate the observed values by about a factor of two. In view of the sensitivity of the form factors for the $0^+ \rightarrow 2_2^+$ transition towards small configurational admixtures, an inclusion of the quasiparticle excitations in the oblate HF state is likely to result in further improvements.

We next present in Fig. IV.2 a comparison of the calculated and experimental[5] results for the nucleus $^{50}$Cr. The shell model results obtained with various effective interactions have also been presented. In the nucleus $^{48}$Ti only the part of the calculated form factor for the $0^+ \rightarrow 2_2^+$ transition involving $q_{eff} > 1.5$ fm$^{-1}$ is found to be sensitive towards the choice of the effective interaction employed in the restricted shell model work. In contrast to this, even the low momentum-transfer part of the restricted shell model estimates for $|F|^2$ $(0^+ \rightarrow 2_2^+)$ displays significant interaction dependence in the nucleus $^{50}$Cr; the $|F|^2$ values resulting from V(Ca-Sc) and V(27-28) differ by more than a factor of 5 throughout the range 0.5 fm$^{-1}$ < $q_{eff}$ < 2.0 fm$^{-1}$. Further, both the interaction V(Ca-Sc) as well as V(27-28) fail to reproduce even qualitatively the observed form factors for the $0^+ \rightarrow 2_2^+$ transition; the magnitude of $|F|^2$ around its second minimum are much too low compared with the experiments.

The use of the projected HFB wave functions for the $2_2^+$ state leads to the required enhancement around the second maximum. One also observes a shift of the dip in the $|F|^2$ values towards the lower momentum-transfer region. Although the PHFB results for the $0^+ \rightarrow 2_2^+$ form factors for $q_{eff} \sim 0.8$ fm$^{-1}$ are still somewhat larger compared to the experiments, the present calculation is seen to yield significant improvement vis-à-vis simultaneous description of the form factors for the

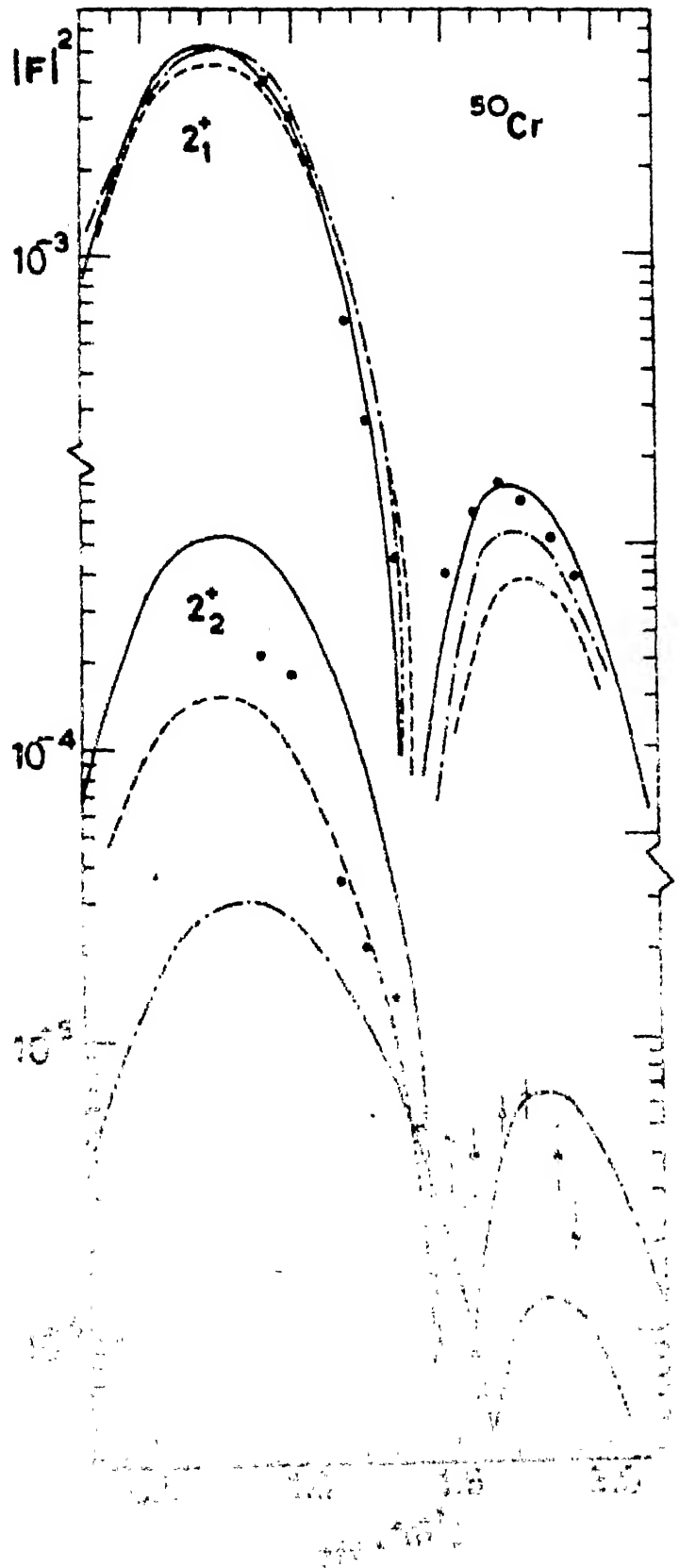


FIG. [illegible] THE EXPERIMENTAL AND CALCULATED SQUARED FORM FACTORS FOR THE $0^+ \rightarrow 2^+$ TRANSITIONS IN $^{50}Cr$

$0^+ \rightarrow 2_1^+$ as well as the $0^+ \rightarrow 2_2^+$ transitions in the nucleus $^{50}Cr$.

It may be mentioned here that the effective charges employed in the earlier calculation, $(e_p, e_n) = (1.6e, 1.2e)$, were also considerably larger than the ones involved in the present calculation. In view of the relatively large values of the calculated intrinsic quadrupole moment (see column 4, Table IV.1), one expects an enhanced involvement of the configurations outside the $(f_{7/2}^n + f_{7/2}^{n-1} p_{3/2})$ space in the nucleus $^{50}Cr$. The increased value of the effective charges employed in the earlier work[5] may be intended to simulate this effect to some extent.

Figure IV.3 presents a comparison of the calculated and the experimental[3] $|F|^2$ for the $0^+ \rightarrow 2_1^+$ and $0^+ \rightarrow 2_2^+$ transitions in the nucleus $^{54}Fe$. Although the present calculation yields an adequate description of the form factors around the first maximum for both the $0^+ \rightarrow 2_1^+$ as well as $0^+ \rightarrow 2_2^+$ transitions, one notices significant discrepancies for $|F|^2$ $(0^+ \rightarrow 2_{1,2}^+)$ for $q_{eff} > 1.4$ fm$^{-1}$. In particular, the value of the form factor for $0^+ \rightarrow 2_2^+$ transition around its second maximum is underestimated by roughly a factor of 6. In view of the smallness of the contribution of the neutrons towards the quadrupole moment of the oblate HF intrinsic state associated with the $2_2^+$ state (see column 4, Table IV.1), the observed discrepancy may be due to insufficient admixture of various shell model configurations involving neutrons.

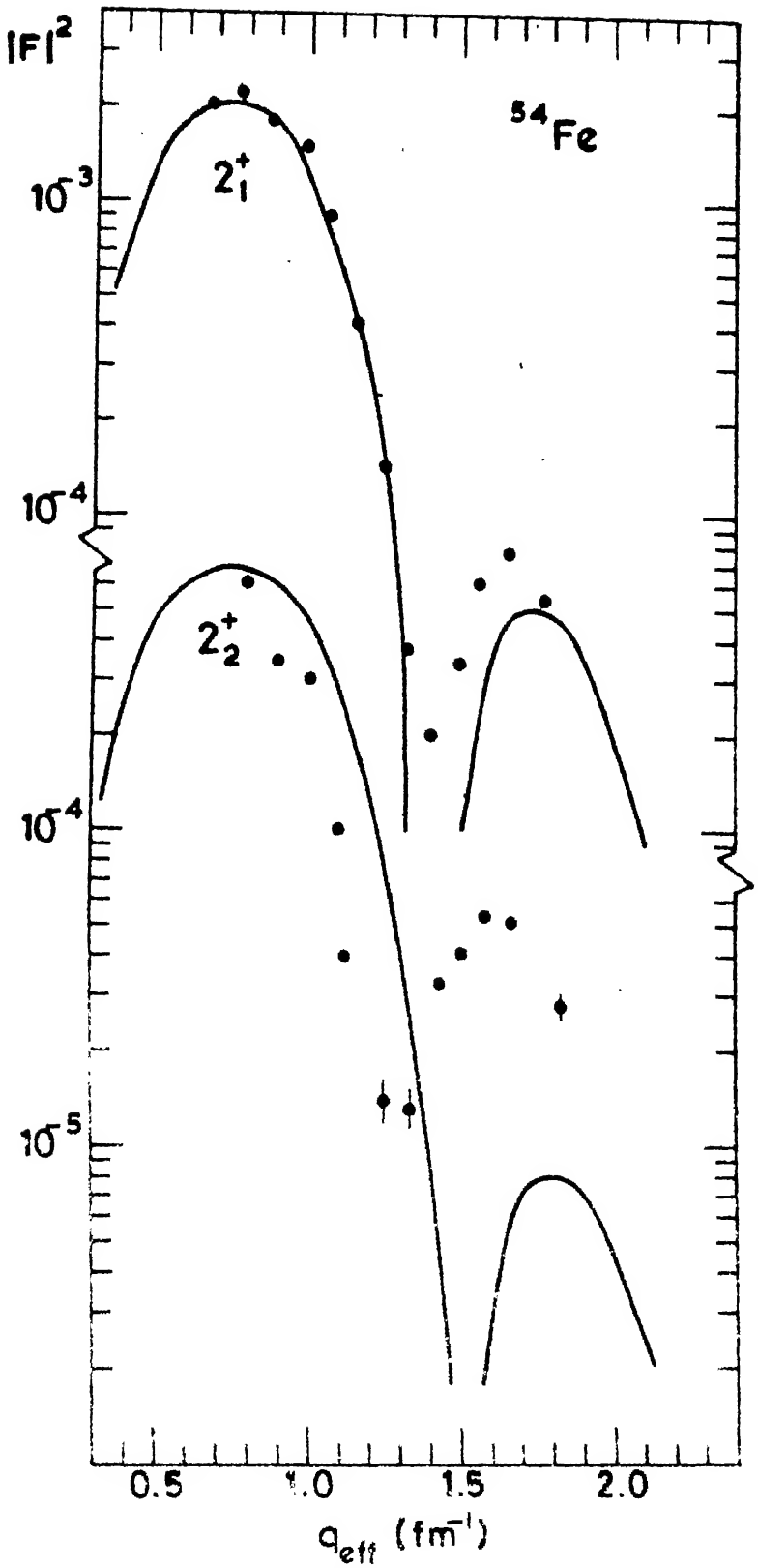


FIG IV.3 THE EXPERIMENTAL AND CALCULATED SQUARED FORM FACTORS FOR THE $0^+ \rightarrow 2^+_{1,2}$ TRANSITIONS IN $^{54}Fe$.

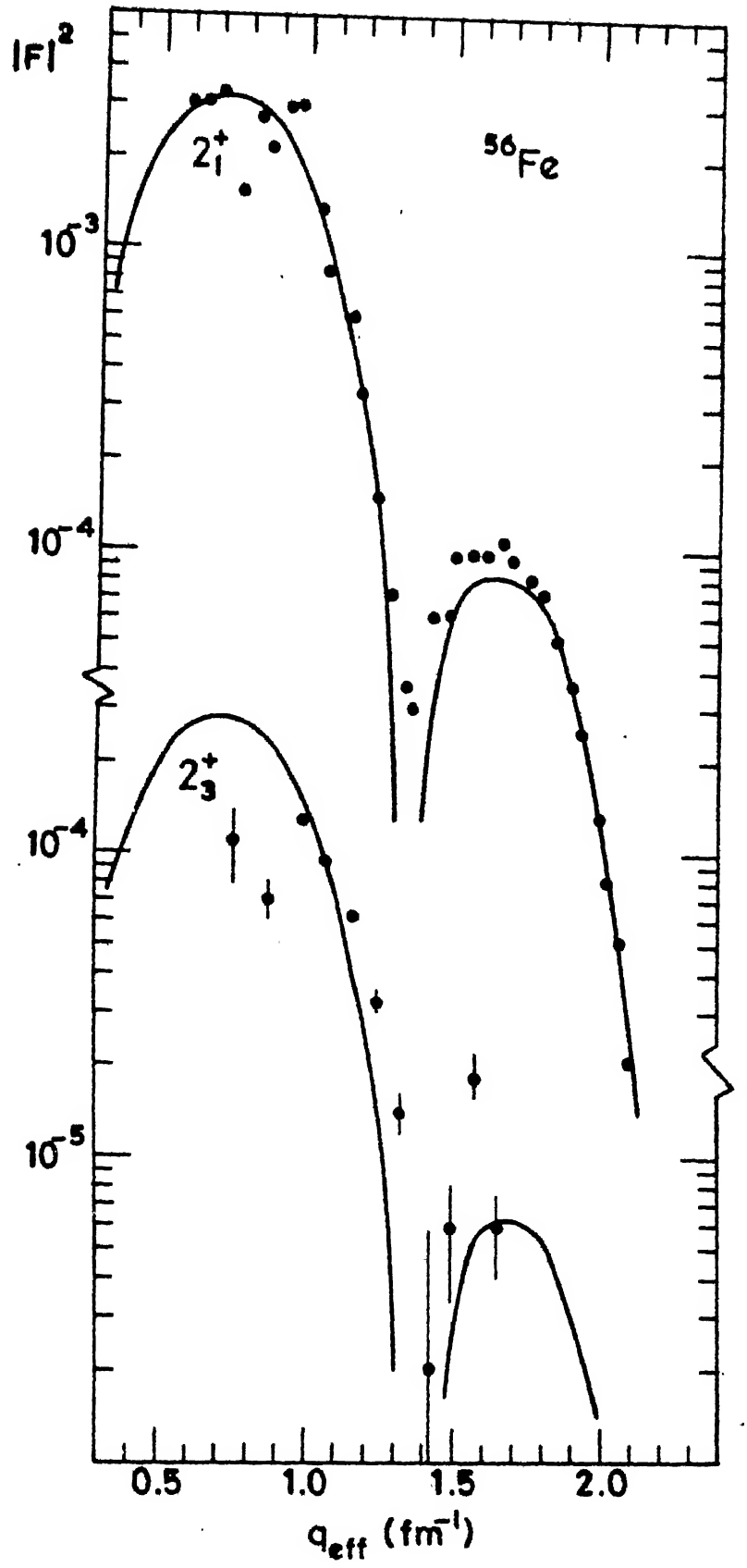


FIG. IV. 4 THE EXPERIMENTAL AND CALCULATED SQUARED FORM FACTORS FOR THE $0^+ \longrightarrow 2^+_{1,3}$ TRANSITIONS IN $^{56}Fe$.

Figure IV.4 compares the calculated and experimental[3,4] form factors for the $0^+ \rightarrow 2_1^+$ and $0^+ \rightarrow 2_3^+$ excitations in the nucleus $^{56}Fe$. It turns out that the present calculation provides acceptable overall quantitative agreement with the available data simultaneously for the $0^+ \rightarrow 2_1^+$ as well as $0^+ \rightarrow 2_3^+$ transitions.

The experimental $|F|^2$ data on $0^+ \rightarrow 2_3^+$ transition for $q > 1.4$ fm$^{-1}$ is characterized by large error bars. Availability of more accurate data for the momentum transfer range $1.5 < q < 2.0$ fm$^{-1}$ will permit a better assessment of the present calculational framework.

## IV.4 Conclusions

Summarizing, we have shown that the use of the yrast, yrare as well as yr $J^\pi = 2^+$ states projected from self-consistent prolate and oblate intrinsic states resulting from the modified KB interaction for the 2p-1f shell permits a reasonably adequate simultaneous description of the observed data involving the $0^+ \rightarrow 2^+_{1,2,3}$ transitions in the nuclei $^{48}Ti$, $^{50}Cr$ and $^{56}Fe$ which possess sizable quadrupole deformation.

As mentioned earlier, an important feature that characterizes the observed form factors for the $0^+ \rightarrow 2^+_{2,3}$ transitions in the nuclei $^{48}Ti$, $^{50}Cr$ and $^{56}Fe$ is their reduced magnitude—by an order of magnitude — compared to

those for the $0^+ \rightarrow 2_1^+$ transitions. Present microscopic description offers a simple qualitative understanding of this feature of the $0^+ \rightarrow 2_{2,3}^+$ transitions in terms of the reduced overlap between the initial ($0^+$) and the final ($2_{2,3}^+$) states due to their different intrinsic parentage.

## REFERENCES


1. J.W. Lightbody, Jr., et al., Bull. Am. Phys. Soc. 20, 568 (1975).
2. A. Hotta et al., Res. Rep. Nucl. Sc., Tohoku Univ. 9, 7 (1976); 10, 18 (1977).
3. K. Hosoyama et al., Res. Rep. Nucl. Sc., Tohoku Univ. 11, 1 (1978).
4. J. Heisenberg, J.S. McCarthy, and I. Sick, Nucl. Phys. A164, 353 (1971).
5. T. Iwamoto, H. Horie, and A. Yokoyama, Phys. Rev. C25, 658 (1982).
6. T. Oda, K. Muto and H. Horie, Lett. Nuovo Cimento, 18, 549 (1977).
7. A. Yokoyama, T. Oda and H. Horie, Prog. Theor. Phys. 60, 427 (1978).
8. T.T.S. Kuo and G.E. Brown, Nucl. Phys. A114, 241 (1968).
9. J.B. McGrory, B.H. Wildenthal and E.C. Halbert, Phys. Rev. C2, 186 (1970).
10. G. Mukherjee and S.K. Sharma, Phys. Rev. C29, 2101 (1984).
11. G. Mukherjee and S.K. Sharma, Phys. Rev. C31, 689 (1985).
12. H. Überall, Electron Scattering from Complex Nuclei (Academic, New York, 1971).

# CHAPTER V

## CONCLUSIONS

Inelastic electron scattering easily surpasses many other methods employed for investigating nuclear structure as far as versatility, possibility of unambiguous interpretation and accuracy is concerned. The nuclear matrix elements extracted from the measurement of the cross section for the inelastic Coulomb scattering can be considered to be the analogs of the usual matrix elements of the electric $2^L$-pole operator at non-zero momentum-transfers. In contrast to the ordinary $\gamma$-transitions, the momentum-transfer dependence of the nuclear matrix elements contains information about the spatial structure of the nuclear states involved and can therefore provide us a good test of the nuclear wave functions.

The work presented in this thesis was motivated primarily by a desire to assess the validity of the projected HFB method in the context of a microscopic discussion of the recent Coulomb form factor data involving the low-lying $2^+$ levels in some 2p-1f shell nuclei; such an assessment is warranted because one is constrained to use the projected HFB method as an alternative to large-scale shell model calculations which are intractable in most of the 2p-1f shell nuclei. Our results indicate that the

calculational framework employed here can be considered fairly reliable for interpreting and correlating the available data on the usual electromagnetic properties — e.g. the static moments and the E2 transition probabilities — as well as the electroexcitation form factors involving low-lying $2^+$ levels.

The results presented in Chapter III have revealed noticeable discrepancies between the calculated and the observed $|F(q)|^2$ values around the second maxima ($q \sim 1.7$ fm$^{-1}$) associated with the $0^+ \rightarrow 2_1^+$ transitions in some nuclei. In this connection it will be worthwhile to examine the application of distorted wave Born approximation (DWBA) instead of the PWBA.

The results presented in Chapter IV indicate that the projected HFB prescription leads to an overestimation of the $0^+ \rightarrow 2_2^+$ form factors around $q \sim 0.7$ fm$^{-1}$ in some cases although the effective charges involved in these transitions are slightly smaller than the ones used for the $0^+ \rightarrow 2_1^+$ transitions. This appears to necessitate an improved description of the yrare $2^+$ levels via an inclusion of some additional quasiparticle-excited configurations.

## APPENDIX A

### THE ($1f_{7/2}$, $2p_{3/2}$, $2p_{1/2}$, $1f_{5/2}$) MATRIX ELEMENTS OF THE KB AS WELL AS THE MWH INTERACTIONS

We tabulate here the matrix elements <abJT|V|cdJT> of the Kuo-Brown (KB) interaction. The columns labelled by (a,b,c,d) contain twice the j-value of the various shell model orbits.

| T | a | b | c | d | J | <\|V\|> | J | <\|V\|> | J | <\|V\|> |
|---|---|---|---|---|---|---|---|---|---|---|
| 1 | 7 | 7 | 7 | 7 | 0 | -1.807 | 2 | -0.785 | 4 | -0.087 |
| | | | | | 6 | 0.226 | | | | |
| 1 | 7 | 7 | 7 | 5 | 2 | 0.000 | 4 | -0.406 | 6 | -0.716 |
| 1 | 7 | 7 | 7 | 3 | 2 | -0.502 | 4 | -0.307 | | |
| 1 | 7 | 7 | 7 | 1 | 4 | -0.293 | | | | |
| 1 | 7 | 7 | 5 | 5 | 0 | -2.788 | 2 | -0.638 | 4 | -0.400 |
| 1 | 7 | 7 | 5 | 3 | 2 | 0.305 | 4 | 0.305 | | |
| 1 | 7 | 7 | 5 | 1 | 2 | -0.470 | | | | |
| 1 | 7 | 7 | 3 | 3 | 0 | -0.783 | 2 | -0.269 | | |
| 1 | 7 | 7 | 3 | 1 | 2 | -0.250 | | | | |
| 1 | 7 | 7 | 1 | 1 | 0 | -0.714 | | | | |
| 1 | 7 | 5 | 7 | 5 | 1 | -0.287 | 2 | -0.096 | 3 | 0.022 |
| | | | | | 4 | 0.031 | 5 | 0.156 | 6 | -0.894 |
| 1 | 7 | 5 | 7 | 3 | 2 | 0.014 | 3 | -0.118 | 4 | -0.114 |
| | | | | | 5 | -0.010 | | | | |
| 1 | 7 | 5 | 7 | 1 | 3 | -0.012 | 4 | -0.093 | | |

| T | a | b | c | d | J | <\|V\|> | J | <\|V\|> | J | <\|V\|> |
|---|---|---|---|---|---|---|---|---|---|---|
| 1 | 7 | 5 | 5 | 5 | 2 | -0.631 | 4 | -0.468 | | |
| 1 | 7 | 5 | 5 | 3 | 1 | -0.035 | 2 | 0.295 | 3 | -0.132 |
| | | | | | 4 | 0.493 | | | | |
| 1 | 7 | 5 | 5 | 1 | 2 | -0.342 | 3 | 0.080 | | |
| 1 | 7 | 5 | 3 | 3 | 2 | -0.018 | | | | |
| 1 | 7 | 5 | 3 | 1 | 1 | -0.079 | 2 | -0.150 | | |
| 1 | 7 | 3 | 7 | 3 | 2 | -0.861 | 3 | -0.027 | 4 | -0.047 |
| | | | | | 5 | 0.145 | | | | |
| 1 | 7 | 3 | 7 | 1 | 3 | 0.078 | 4 | -0.502 | | |
| 1 | 7 | 3 | 5 | 5 | 2 | -0.446 | 4 | -0.156 | | |
| 1 | 7 | 3 | 5 | 3 | 2 | 0.402 | 3 | 0.026 | 4 | 0.619 |
| 1 | 7 | 3 | 5 | 1 | 2 | -0.966 | 3 | -0.059 | | |
| 1 | 7 | 3 | 3 | 3 | 2 | -0.325 | | | | |
| 1 | 7 | 3 | 3 | 1 | 2 | -0.319 | | | | |
| 1 | 7 | 1 | 7 | 1 | 3 | 0.029 | 4 | -0.274 | | |
| 1 | 7 | 1 | 5 | 5 | 4 | -0.252 | | | | |
| 1 | 7 | 1 | 5 | 3 | 3 | 0.140 | 4 | 0.531 | | |
| 1 | 7 | 1 | 5 | 1 | 3 | -0.078 | | | | |
| 1 | 5 | 5 | 5 | 5 | 0 | -0.860 | 2 | -0.218 | 4 | 0.298 |
| 1 | 5 | 5 | 5 | 3 | 2 | 0.023 | 4 | 0.102 | | |
| 1 | 5 | 5 | 5 | 1 | 2 | -0.186 | | | | |
| 1 | 5 | 5 | 3 | 3 | 0 | -0.777 | 2 | -0.128 | | |
| 1 | 5 | 5 | 3 | 1 | 2 | -0.256 | | | | |
| 1 | 5 | 5 | 1 | 1 | 0 | -0.392 | | | | |

| T | a | b | c | d | J | $\langle \lvert V \rvert \rangle$ | J | $\langle \lvert V \rvert \rangle$ | J | $\langle \lvert V \rvert \rangle$ |
|---|---|---|---|---|---|---|---|---|---|---|
| 1 | 5 | 3 | 5 | 3 | 1 | -0.032 | 2 | 0.215 | 3 | 0.120 |
| | | | | | 4 | -0.243 | | | | |
| 1 | 5 | 3 | 5 | 1 | 2 | 0.389 | 3 | 0.007 | | |
| 1 | 5 | 3 | 3 | 3 | 2 | 0.068 | | | | |
| 1 | 5 | 3 | 3 | 1 | 1 | -0.058 | 2 | 0.159 | | |
| 1 | 5 | 1 | 5 | 1 | 2 | -0.135 | 3 | 0.205 | | |
| 1 | 5 | 1 | 3 | 3 | 2 | -0.047 | | | | |
| 1 | 5 | 1 | 3 | 1 | 2 | -0.241 | | | | |
| 1 | 3 | 3 | 3 | 3 | 0 | -1.206 | 2 | -0.380 | | |
| 1 | 3 | 3 | 3 | 1 | 2 | -0.601 | | | | |
| 1 | 3 | 3 | 1 | 1 | 0 | -1.465 | | | | |
| 1 | 3 | 1 | 3 | 1 | 1 | 0.152 | 2 | -0.688 | | |
| 1 | 1 | 1 | 1 | 1 | 0 | -0.249 | | | | |
| 0 | 7 | 7 | 7 | 7 | 1 | -0.525 | 3 | -0.208 | 5 | -0.502 |
| | | | | | 7 | -2.199 | | | | |
| 0 | 7 | 7 | 7 | 5 | 1 | 1.894 | 3 | 1.005 | 5 | 0.901 |
| 0 | 7 | 7 | 7 | 3 | 3 | -0.482 | 5 | -0.816 | | |
| 0 | 7 | 7 | 7 | 1 | 3 | 0.640 | | | | |
| 0 | 7 | 7 | 5 | 5 | 1 | 1.071 | 3 | 0.517 | 5 | 0.170 |
| 0 | 7 | 7 | 5 | 3 | 1 | 0.227 | 3 | -0.087 | | |
| 0 | 7 | 7 | 5 | 1 | 3 | 0.033 | | | | |
| 0 | 7 | 7 | 3 | 3 | 1 | -0.279 | 3 | -0.296 | | |
| 0 | 7 | 7 | 3 | 1 | 1 | 0.392 | | | | |
| 0 | 7 | 7 | 1 | 1 | 1 | 0.184 | | | | |

| T | a | b | c | d | J | <\|v\|> | J | <\|v\|> | J | <\|v\|> |
|---|---|---|---|---|---|---|---|---|---|---|
| 0 | 7 | 5 | 7 | 5 | 1 | -3.621 | 2 | -2.731 | 3 | -0.985 |
| | | | | | 4 | -1.886 | 5 | -0.112 | 6 | -2.217 |
| 0 | 7 | 5 | 7 | 3 | 2 | -0.735 | 3 | 0.328 | 4 | -0.039 |
| | | | | | 5 | 0.405 | | | | |
| 0 | 7 | 5 | 7 | 1 | 3 | -0.440 | 4 | -0.674 | | |
| 0 | 7 | 5 | 5 | 5 | 1 | -0.416 | 3 | 0.675 | 5 | 1.138 |
| 0 | 7 | 5 | 5 | 3 | 1 | 0.953 | 2 | -0.705 | 3 | 0.628 |
| | | | | | 4 | -0.544 | | | | |
| 0 | 7 | 5 | 5 | 1 | 2 | 0.427 | 3 | 0.539 | | |
| 0 | 7 | 5 | 3 | 3 | 1 | 0.871 | 3 | 0.538 | | |
| 0 | 7 | 5 | 3 | 1 | 1 | -1.449 | 2 | -0.659 | | |
| 0 | 7 | 5 | 1 | 1 | 1 | 0.168 | | | | |
| 0 | 7 | 3 | 7 | 3 | 2 | -0.293 | 3 | -0.604 | 4 | -0.164 |
| | | | | | 5 | -2.165 | | | | |
| 0 | 7 | 3 | 7 | 1 | 3 | 1.295 | 4 | 0.108 | | |
| 0 | 7 | 3 | 5 | 5 | 3 | 0.158 | 5 | 0.048 | | |
| 0 | 7 | 3 | 5 | 3 | 2 | -1.123 | 3 | -0.408 | 4 | -0.614 |
| 0 | 7 | 3 | 5 | 1 | 2 | 0.838 | 3 | 0.518 | | |
| 0 | 7 | 3 | 3 | 3 | 3 | -0.511 | | | | |
| 0 | 7 | 3 | 3 | 1 | 2 | -0.481 | | | | |
| 0 | 7 | 1 | 7 | 1 | 3 | -1.484 | 4 | -0.746 | | |
| 0 | 7 | 1 | 5 | 5 | 3 | -0.270 | | | | |
| 0 | 7 | 1 | 5 | 3 | 3 | 0.139 | 4 | -1.188 | | |
| 0 | 7 | 1 | 5 | 1 | 3 | 0.400 | | | | |
| 0 | 7 | 1 | 3 | 3 | 3 | 0.461 | | | | |

| T | a | b | c | d | J | $\langle \lvert V \rvert \rangle$ | J | $\langle \lvert V \rvert \rangle$ | J | $\langle \lvert V \rvert \rangle$ |
|---|---|---|---|---|---|---|---|---|---|---|
| 0 | 5 | 5 | 5 | 5 | 1 | -0.012 | 3 | -0.196 | 5 | -1.687 |
| 0 | 5 | 5 | 5 | 3 | 1 | -0.292 | 3 | -0.327 | | |
| 0 | 5 | 5 | 5 | 1 | 3 | -0.391 | | | | |
| 0 | 5 | 5 | 3 | 3 | 1 | 0.040 | 3 | -0.182 | | |
| 0 | 5 | 5 | 3 | 1 | 1 | 0.159 | | | | |
| 0 | 5 | 5 | 1 | 1 | 1 | -0.084 | | | | |
| 0 | 5 | 3 | 5 | 3 | 1<br>4 | -2.164<br>-0.722 | 2 | -1.236 | 3 | -0.459 |
| 0 | 5 | 3 | 5 | 1 | 2 | 0.255 | 3 | -0.988 | | |
| 0 | 5 | 3 | 3 | 3 | 1 | -0.073 | 3 | -0.340 | | |
| 0 | 5 | 3 | 3 | 1 | 1 | 0.620 | 2 | -0.071 | | |
| 0 | 5 | 3 | 1 | 1 | 1 | -0.393 | | | | |
| 0 | 5 | 1 | 5 | 1 | 2 | -0.081 | 3 | -1.234 | | |
| 0 | 5 | 1 | 3 | 3 | 3 | -0.084 | | | | |
| 0 | 5 | 1 | 3 | 1 | 2 | 0.464 | | | | |
| 0 | 3 | 3 | 3 | 3 | 1 | -0.639 | 3 | -1.832 | | |
| 0 | 3 | 3 | 3 | 1 | 1 | 1.554 | | | | |
| 0 | 3 | 3 | 1 | 1 | 1 | 0.709 | | | | |
| 0 | 3 | 1 | 3 | 1 | 1 | -2.291 | 2 | -1.897 | | |
| 0 | 3 | 1 | 1 | 1 | 1 | 0.686 | | | | |
| 0 | 1 | 1 | 1 | 1 | 1 | -1.074 | | | | |

The MWH interaction referred to in the thesis is obtained from the KB interaction by substituting the following matrix elements in place of their counterparts.

| T | a | b | c | d | J | $\langle \lvert V \rvert \rangle$ | J | $\langle \lvert V \rvert \rangle$ | J | $\langle \lvert V \rvert \rangle$ |
|---|---|---|---|---|---|---|---|---|---|---|
| 1 | 7 | 7 | 7 | 7 | 0 | -2.107 | 2 | -1.115 | 4 | -0.097 |
| 1 | 7 | 5 | 7 | 5 | 1 | -0.037 | 2 | 0.154 | 3 | 0.272 |
| | | | | | 4 | 0.281 | 5 | 0.406 | 6 | -0.644 |
| 1 | 7 | 3 | 7 | 3 | 2 | -0.561 | 3 | 0.253 | 4 | 0.283 |
| | | | | | 5 | 0.485 | | | | |
| 1 | 7 | 1 | 7 | 1 | 3 | 0.279 | 4 | -0.024 | | |